The Canadian Mineralogist
Vol. 42, pp. 325-350 (2004)

THE AGUABLANCA Ni–Cu–PGE DEPOSIT, SOUTHWESTERN IBERIA: MAGMATIC ORE-FORMING PROCESSES AND RETROGRADE EVOLUTION

LORENA ORTEGA[§] AND ROSARIO LUNAR

Departamento de Cristalografía y Mineralogía, C.C. Geológicas, Universidad Complutense, E–28040 Madrid, Spain

FÉLIX GARCÍA-PALOMERO

Atlantic Copper S.A., Av. Francisco Montegro s/n, E–21001 Huelva, Spain

TERESA MORENO

Department of Earth, Ocean and Planetary Sciences, University of Cardiff, Cardiff CF10 3YE, U.K.

JOSÉ RAMÓN MARTÍN-ESTÉVEZ

Departamento de Cristalografía y Mineralogía, C.C. Geológicas, Universidad Complutense, E–28040 Madrid, Spain

HAZEL M. PRICHARD and PETER C. FISHER

Department of Earth, Ocean and Planetary Sciences, University of Cardiff, Cardiff CF10 3YE, U.K.

ABSTRACT

The Aguablanca Ni–Cu–PGE ore deposit, in southwestern Iberia, has a magmatic origin, and has been reworked by later skarn-related hydrothermal activity. Base-metal sulfides are associated with igneous cumulates displaying subvertical layering consisting of gabbro, norite and dolerite, with fragments of pyroxenite and peridotite. These rocks show a pervasive retrograde alteration with an early overprint of actinolite ± chlorite ± epidote ± albite ± serpentine, followed by later growth of talc ± chlorite ± carbonates. The base-metal sulfides are concentrated in two subvertical bodies and consist of pyrrhotite, pentlandite and chalcopyrite, overprinted by fluid-deposited pyrite. The following types of mineralization have been recognized: 1) disseminated ore ($1 < Ni/Cu < 1.5$), with sulfides occurring interstitially to the igneous silicates, 2) semimassive to massive ore ($2 < Ni/Cu < 5$), with net-textured to poikilitic sulfides, 3) breccia ore, consisting of fragments of unmineralized ultramafic rocks in a massive sulfide matrix, 4) nodules of sulfides, 5) pyrrhotite veinlets, and 6) chalcopyrite veinlets. The PGE content and (Pt + Pd):(Ru + Ir + Os) ratio have their highest values in the Cu-rich disseminated ore and associated veinlets of chalcopyrite. The platinum-group minerals (PGM) associated with the base-metal sulfides at Aguablanca include michenerite, merenskyite, moncheite, palladian melonite and sperrylite. These mostly occur enclosed within sulfide minerals or close to contacts between them. The PGE tellurides show an extensive substitution of Bi for Te, indicating temperatures of formation below 500°C. A PGE oxide assemblage has also been discovered in samples from the surface gossan developed above the sulfides. The composition of the PGM and their association with magmatic base-metal sulfides suggest that they exsolved from the sulfides during subsolidus recrystallization, although some remobilization may have occurred in areas of pervasive circulation of fluid.

Keywords: Ni–Cu sulfides, platinum-group minerals, PGE oxides, tellurides, magmatic ore, retrograde alteration, Variscan, Aguablanca, Spain.

SOMMAIRE

Le gisement à Ni–Cu–EGP (éléments du groupe du platine) d'Aguablanca, dans le sud-ouest de la péninsule ibérique, possède une origine magmatique, mais il a subi une activité hydrothermale liée à la formation de skarns. Les sulfures des métaux de base sont associés aux cumulats ignés dont le litage est subvertical, les roches dominantes étant gabbro, norite et dolérite, avec des fragments de pyroxénite et de péridotite. Ces roches font preuve d'une rétrogression répandue, d'abord à l'assemblage actinolite ± chlorite ± épidote ± albite ± serpentine, suivi de l'assemblage talc ± chlorite ± carbonates. Les sulfures des métaux de base sont

§ *E-mail address*: lortega@geo.ucm.es

concentrés dans deux accumulations subverticales de pyrrhotite, pentlandite et chalcopyrite, avec pyrite tardive hydrothermale. Nous distinguons les types de minéralisation suivants: 1) minerai disséminé ($1 < Ni/Cu < 1.5$), les sulfures étant distribués de façon interstitielle par rapport aux silicates ignés, 2) minerai semi-massif à massif ($2 < Ni/Cu < 5$), les sulfures définissant un réseau ou des amas poecilitiques, 3) minerai bréchique, contenant des fragments de roches ultramafiques non minéralisées dans une matrice de sulfures massifs, 4) des nodules de sulfures, 5) des veinules de pyrrhotite, et 6) des veinules de chalcopyrite. Les teneurs en EGP et le rapport (Pt + Pd):(Ru + Ir + Os) atteignent leurs valeurs les plus élevées dans le minerai disséminé enrichi en cuivre et dans les veinules de chalcopyrite qui lui sont associées. Parmi les minéraux du groupe du platine associés aux métaux de base sont michenerite, merenskyite, monchéite, melonite palladifère et sperrylite. Ces minéraux se présentent surtout en inclusions dans les sulfures ou près des contacts entre ces grains de sulfures. Les tellurures des EGP font preuve d'une substitution importante du Bi pour le Te, indication d'une température de cristallisation inférieure à 500°C. Un assemblage d'oxydes des EGP a de plus été découvert dans les chapeaux de fer en surface, développés aux dépens des amas de sulfures. La composition des minéraux du groupe du platine et leur association avec les sulfures des métaux de base magmatiques font penser qu'ils se sont formés par exsolution des sulfures au cours de la recristallisation subsolidus, quoiqu'une partie de la remobilisation est bien sûr attribuable à la circulation répandue de fluides.

(Traduit par la Rédaction)

Mots-clés: sulfures de Ni–Cu, minéraux du groupe du platine, oxydes des éléments du groupe du platine, tellurures, minerai magmatique, altération rétrograde, Varisque, Aguablanca, Espagne.

Introduction

There are a number of occurrences of platinum-group-element (PGE) mineralization in the Iberian Peninsula, including Cabo Ortegal (Moreno *et al*. 2001), Bragança (Bridges *et al*. 1993) and the Ronda Massif (Gervilla & Leblanc 1990); these are associated with concentrations of chromite. In contrast, the concentrations of PGE in the Aguablanca deposit are associated with massive and disseminated Ni–Cu sulfides that are chromite-poor. The deposit, located at 37°57'51''N and 6°11'41''W, was discovered in 1993 (Lunar *et al*. 1997, Ortega *et al*. 2000), and is the only one known in Iberia of sufficient tonnage to be economically viable. The sulfide mineralization, mainly composed of pyrrhotite, pentlandite, chalcopyrite and pyrite, is associated with the mafic and ultramafic rocks that form the Aguablanca intrusion. Such Ni–Cu mineralization associated with mafic intrusions is not common in Europe: known examples include in the Vammala, Hitura and Kotalahti complexes in Finland (Frietsch *et al*. 1979, Häkli *et al*. 1979, Gervilla *et al*. 1998), Råna in Norway (Boyd & Mathiesen 1979) and Ivrea–Verbano in Italy (Garuti & Rinaldi 1986a, b, Garuti *et al*. 1986). However, the discovery of Aguablanca has promoted one of the most comprehensive and systematic reconnaissance programs ever attempted in the Iberian Peninsula, carried out by the owner company, Rio Narcea Gold Mines (Forrest 2003). By 2002, this exploration program had led to the identification of more than 100 radiometric anomalies similar to that at Aguablanca, one third of these targets having favorable mafic to ultramafic intrusive rocks. Thus the potential of southwestern Iberia will likely modify the outlook of the nickel and PGE supply within Europe in the near future.

The Aguablanca deposit was discovered by Presur – Atlantic Copper S.A. (a joint venture between the Spanish State company Presur and Atlantic Copper S.A., formerly Rio Tinto Minera S.A.) during a gold exploration program. A regional exploration survey carried out by Presur found a nickel anomaly related to a gossan developed on altered gabbros. Short (less than 5 m) vertical percussion drilling and long (up to 550 m) 45° dip diamond coring were carried out by Atlantic Copper S.A. to trace the downward extension of the observed oxidized cap and to identify the extent of the sulfide mineralization. Drilling to date has revealed the existence of two subvertical mineralized bodies containing ore reserves of 31 Mt grading 0.6–0.7% Ni, 0.5–0.6% Cu, 0.02% Co and 0.75 g/t Pt + Pd + Au. Since July 2001, Aguablanca is the property of Rio Narcea Gold Mines S.A., which plans to start mining operations early in 2004.

Previous investigators (Lunar *et al.* 1997, Casquet *et al*. 1998a, Bomatí *et al.* 1999, Ortega *et al*. 1999, 2000, Tornos *et al*. 1999, 2001) presented geological, mineralogical, geochemical and isotopic data on the Aguablanca deposit based on the examination of a few drill-core samples. Our aim in this paper is to present the results of a more detailed examination of the external and internal features of the deposit, taken from the study of cores obtained from the extensive drilling carried out by Atlantic Copper S.A. The data presented below are based on information gained from vertical N–S transverse sections (every 25 m) and horizontal sections (every 50 m) constructed using geological, mineralogical and geochemical data from 30,000 m of core, 6,000 analyses of samples for Cu, Ni and S, and 1,200 analyses of samples for Pt, Pd, Au and Co. Initial mineralogical studies are presented, particularly for the platinum-group minerals (PGM), and the data are interpreted to provide a genetic working hypothesis for the deposit. It is expected that the imminent mining operations will provide an opportunity to gather further information, which will allow refinement of our current understanding of the Aguablanca ores.

Geological Framework

The Aguablanca deposit is located in the Ossa Morena Zone of the Iberian Massif, the westernmost belt of the European Variscan chain (Lunar *et al*. 2002). This zone comprises a Precambrian basement deformed during the Neoproterozoic Cadomian orogeny (620–480 Ma), and Cambrian to Lower Permian sequences affected by the Late Paleozoic Variscan orogeny (390–300 Ma) (Quesada 1992, Eguiluz *et al*. 2000, Valladares *et al*. 2002, and references therein). At least three major igneous events took place during the geodynamic evolution of the area (Sánchez Carretero *et al.* 1990, Quesada 1996, Eguiluz *et al.* 2000, Valladares *et al*. 2002, Sánchez-García *et al.* 2003). The Cadomian orogeny in the Ossa Morena Zone involved the generation of a calc-alkaline volcanic arc in an Andean-type continental margin, with deposition of volcanosedimentary sequences. The Variscan cycle began with an extensional event accompanied by bimodal magmatism with plutonic, subvolcanic and volcanic rocks of alkaline and tholeiitic affinities. Finally, magmatism linked to the Variscan orogeny was characterized by a large volume of post-collisional calc-alkaline plutonic rocks.

The Aguablanca ore-bearing igneous body is a small asymetrically zoned intrusion of tholeiitic affinity composed of gabbroic rocks with ultramafic enclaves in the northern part that grade into amphibole–biotite diorite to the south. The intrusion was emplaced into a volcanic-sedimentary sequence with dominant K-rich rhyolitic units (the Bodonal–Cala Complex of 515 Ma, Oschsner 1993, Ordoñez *et al.* 1998) grading toward the top into Lower Cambrian terrigenous and carbonate sequences (Apalategui *et al.* 1990, Apalategui & Sánchez Carretero 1991) (Fig. 1). The latter carbonate rocks crop out along the northern border of the Aguablanca intrusion, where they are metamorphosed to skarns (garnetites, calc-silicate rocks and marbles) along the contact (Fig. 1). The country rocks are also affected by a regional Variscan greenschist-facies metamorphism. To the south, Aguablanca is intruded by the Santa Olalla pluton (Fig. 1), a calc-alkaline intrusion composed of tonalitic and granodioritic rocks.

The age of Aguablanca and its spatial and temporal relationship to Santa Olalla are matters of debate. Until the discovery of the Aguablanca sulfide deposit, both the Aguablanca and Santa Olalla intrusions were considered to be part of the so-called Santa Olalla Plutonic Complex, forming either two separate, although temporally related intrusions (Casquet 1980, Casquet *et al*. 1998a), or forming different facies of a single asymmetrically zoned pluton (Eguiluz *et al.*1989, Bateman

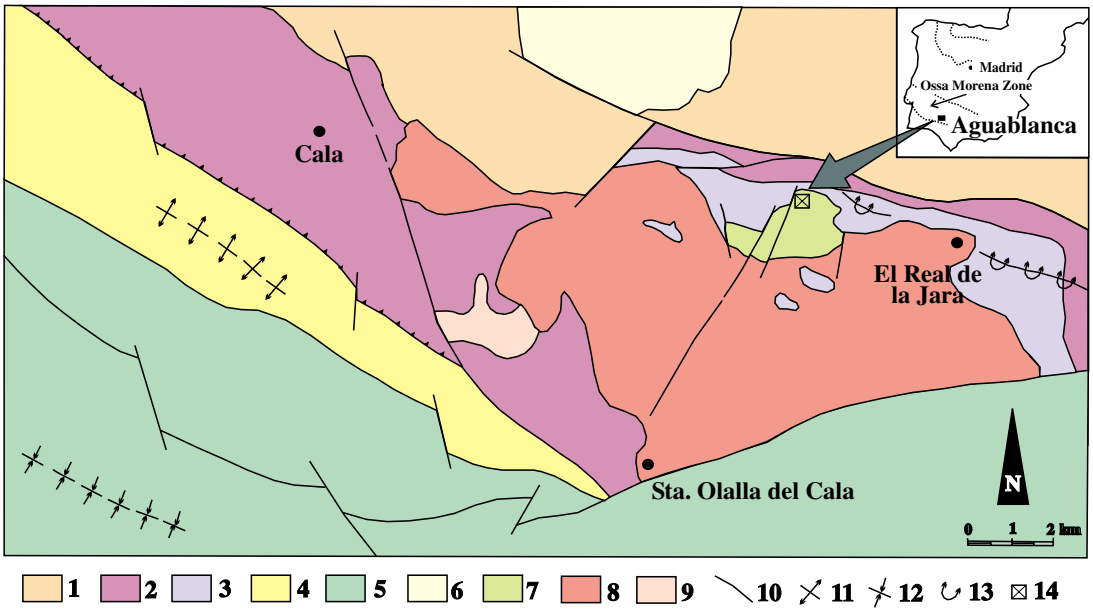

FIG. 1. Geological location of the Aguablanca Ni–Cu–PGE ore deposit. 1. Greywacke and slate (Riphean). 2. Slate and metavolcanic rocks (Upper Riphean – Lower Cambrian, Bodonal–Cala complex). 3. Marble, limestones, skarn, hornfels and garnetites (Upper Riphean – Lower Cambrian). 4. Limestone and slate (Lower Cambrian – Lower Ordovician). 5. Slate, microconglomerate and greywacke (Devonian – Lower Carboniferous). 6. Granite. 7. Aguablanca gabbro and diorite. 8. Santa Olalla tonalite. 9. Alkaline granite. 10. Fault. 11. Anticline. 12. Syncline. 13. Overturned anticline. 14. Aguablanca mineralization. Based on Apalategui *et al*. (1990).

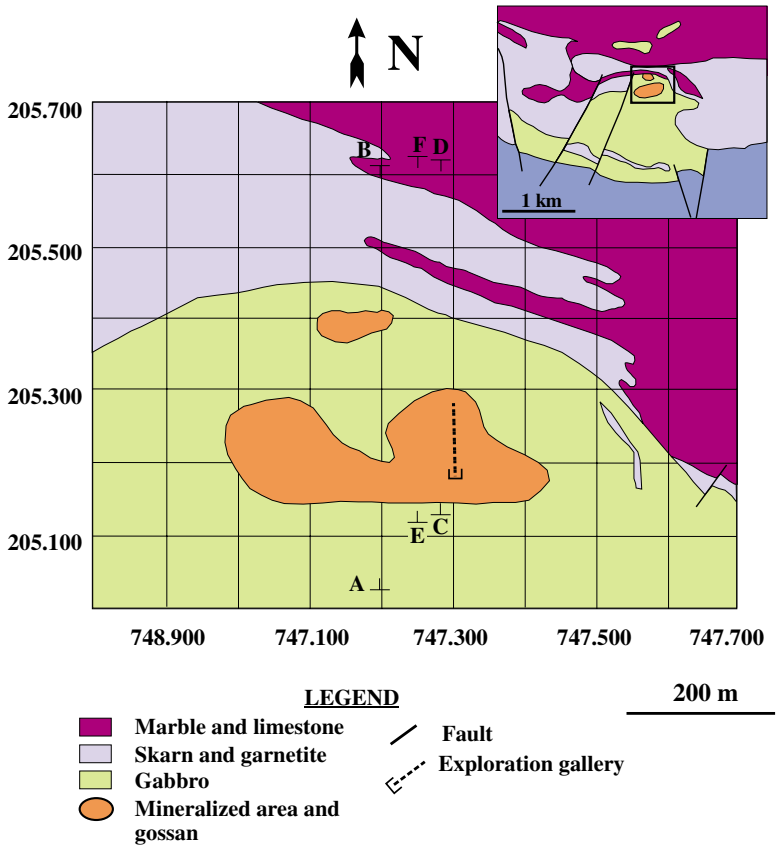

FIG. 2. The Aguablanca intrusion (inset) and location of the outcrops of gossan over the orebodies near the northern border of the intrusion. A–B, C–D and E–F refer to cross-sections in Figures 3, 7A and 7B, respectively.

et al. 1992). There is a general agreement that the Santa Olalla pluton belongs to a group of calc-alkaline Paleozoic intrusions cropping out in the region (Castro *et al.* 2002), and that its age is likely to be similar to those determined for the other plutons (*e.g.*, Burguillos del Cerro, 338 Ma, U/Pb, Casquet *et al.* 1998b). These plutons represent magmatism linked to the Variscan thickening of the crust (Sánchez Carretero *et al.* 1990).

Preliminary studies of the geological features of the sulfide deposit (Lunar *et al.* 1997, Ortega *et al.* 2001) suggested that Aguablanca could be significantly older than Santa Olalla and emplaced before the Variscan episode of deformation. Definitive conclusions cannot be drawn in the absence of radiometric dating. However, the possibility cannot be discarded that the Aguablanca deposit is related to the Cambrian rifting event documented in the region (Quesada 1996, Sánchez-García *et al.* 2003). Thus the Aguablanca intrusion could be one of the rift-related laccolithic plutons covered by the Lower Cambrian carbonate unit, and commonly associated with skarns caused by the emplacement of these plutons (Sánchez-García *et al.* 2003). This geodynamic context would be more consistent with observed relationships than one envisaging a Variscan scenario, as many magmatic sulfide deposits elsewhere in the world occur in rift environments [Lesher 2003, *e.g.*, Noril'sk: Distler & Kunilov (1994); the Duluth Complex: Hauck *et al.* (1997); Pechenga: Lesher & Keays (2002), Melezhik *et al.* (1994)].

THE AGUABLANCA ORE DEPOSIT

The host rocks

The sulfide mineralization is located at the northern margin of the Aguablanca intrusion and is hosted by a E–W-trending subvertical sheet 500 m wide, that thins out laterally. This sheet consists of subvertical layers of norite, gabbronorite, gabbro and dolerite (Figs. 2, 3) and commonly includes igneous enclaves, centimetric in

size, of troctolite, olivine gabbro, pyroxenite, anorthosite and fine-grained norite and gabbro. The contact with the country rocks is intrusive, and in detail both banded and chilled margins have been observed. The internal magmatic layers dip at 70–80%N, which is parallel to the bedding in the metasedimentary host sequence (Figs. 3, 4).

The mafic and ultramafic rocks show primary assemblages of silicates, with cumulus textures overprinted by retrograde metamorphism and alteration. Both norite and gabbro have a variable content of mafic minerals, from about 95 to 20%, ranging from melagabbro and melanorite to much more felsic lithologies. The mineralogy consists mostly of enstatite and augite as cumulus phases, with coarse-grained intercumulus plagioclase. In some rocks, the intercumulus matrix also includes poikilitic hornblende and phlogopite. Disseminated sulfides occur interstitially to the silicate minerals, mostly in the noritic units (Fig. 5A), usually being more abundant (semi-massive to massive) in the melanorite and melagabbronorite units. The peridotite and pyroxenite enclaves preferentially occur within the more mafic norite and gabbro layers, and consist of cumulus olivine and pyroxene with intercumulus plagioclase and minor amphibole. Composite enclaves composed of two layers of pyroxenite and peridotite forming cumulates also have been observed, indicating the presence of a layered ultramafic sequence. In addition, a continuous layer of pyroxenite has been intersected at depth (more than 700 m deep) during recent drilling (Rio Narcea,

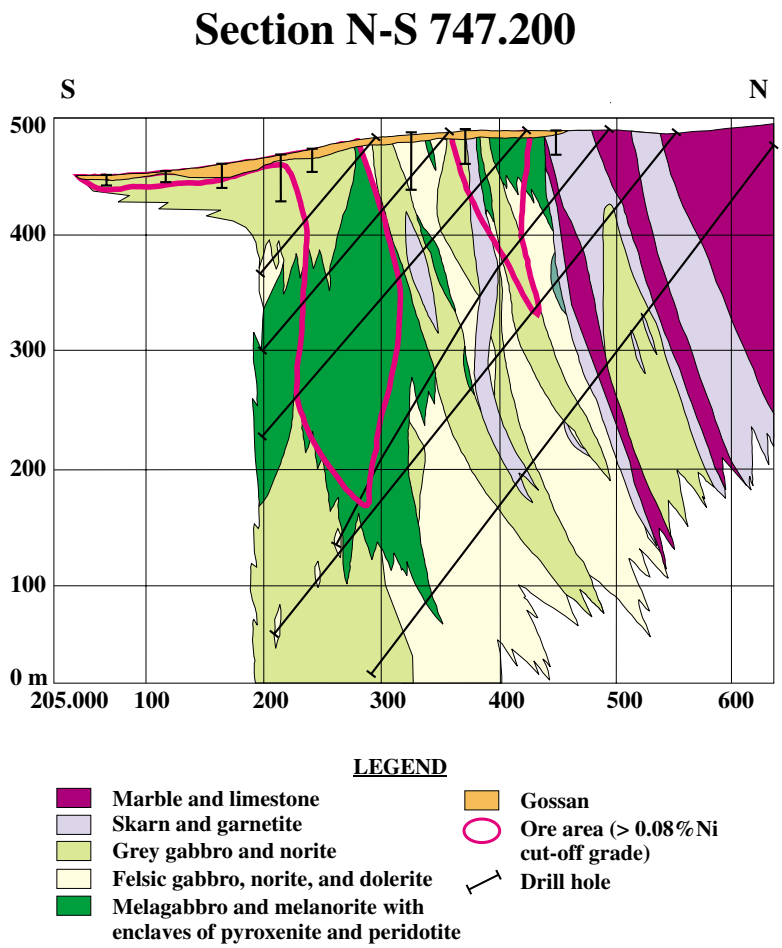

FIG. 3. Geology and outline of the orebodies (Ni > 0.08%) in north–south cross-section 747.200 (A–B in Fig. 2), showing the internal structure of the northern border of the Aguablanca orebody and host rocks. Rock types are labeled with field terms, and the drawing has been constructed from drill-hole information.

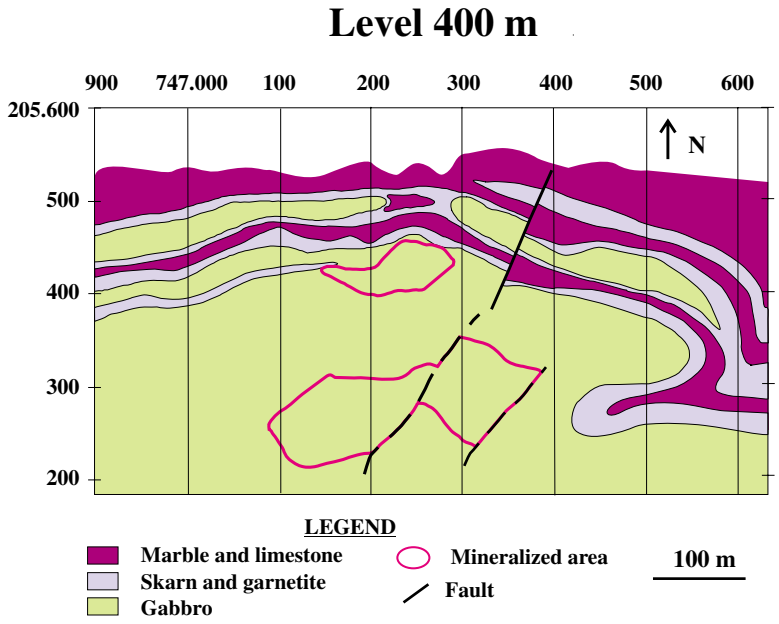

FIG. 4. Geological features of the ore deposit in the horizontal plane at level 400 m, drawn from drill-hole information.

pers. commun.). The enclaves themselves lack sulfides, although they are usually hosted by lithological units containing massive sulfides (Fig. 5B) and are cross-cut by chalcopyrite veinlets.

The igneous rocks show a pervasive retrograde alteration that can be locally very intense. The clinopyroxene is variably altered to actinolite–tremolite and may be completely replaced (Figs. 5C, D). This alteration is locally overprinted by talc–carbonate aggregates (Fig. 5D). The orthopyroxene remains almost unaltered, but is locally partially replaced by anthophyllite or can be almost completely altered to talc. The core of plagioclase grains is mostly transformed to an epidote (or zoisite) + albite + white mica + calcite assemblage. Both pyroxene and plagioclase are locally cut by fractures infilled with talc ± chlorite ± carbonate. In addition, aggregates of coarse chlorite and epidote develop in the more leucocratic gabbros. Serpentinization is mostly restricted to the ultramafic enclaves, in which olivine and pyroxene show variable alteration, which becomes more intense close to fractures. Serpentine is locally overprinted by aggregates of chlorite + talc.

The sulfide ores

Sulfide mineralization occurs very close to the contact with the metasedimentary country-rocks within two subvertical bodies of differing size that dip 80°N and that strike east–west (Figs. 3, 4). The orebodies consist of sulfide-bearing norite, gabbronorite, gabbro and dolerite that grade progressively into sulfide-barren rocks. The outline of the orebodies has been defined by a cut-off grade of 0.08% Ni. Thus the northern orebody is about 30 × 150 m thick and 200 m deep, whereas the southern body, the main one, has an average thickness of 60–100 m (N–S), is 450–500 m in length (E–W), and extends to at least a depth of 700 m (Figs. 3, 4). In this southern body, the sulfide mineralization thins out rapidly to the east, whereas the northwestern limit of the body is marked by a southeasterly dipping planar discontinuity, probably a fault, at which the sulfide mineralization ends abruptly. Late faults cross-cut and displace the ore at different depths, and intense microfracturing is observed in different parts of the ore. A gossan zone, up to 8–10 m thick, is developed where oxidation has taken place.

The following types of mineralization have been recognized (Figs. 5, 6, 7):

1) Disseminated ore ($1 < Ni/Cu < 1.5$) consists of sulfides occurring interstitially to the igneous silicates (Figs. 5A, 6A). This is the dominant type of mineralization in both orebodies (Fig. 7A).

2) Semi-massive to massive ore ($2 < Ni/Cu < 5$), with sulfides making up to the 85% of the rock (Fig. 6B), develop net to poikilitic textures. This mineralization is concentrated in elongate pods striking east–west

and dipping 70°N in the core and northern part of the southern orebody (Fig. 7A). This type of ore accounts for 10–15% of the total reserves (1–1.5 $\times$ 10^6 m^3 of mineralized rocks).

3) Breccia ore (*mineralized breccia* in Tornos *et al.* 2001) consists of rounded fragments of unmineralized pyroxenite and peridotite in a massive sulfide matrix (Figs. 5B, 6C). The rounded shape of the fragments and the lack of sharp contacts between them and the massive sulfide-bearing rocks suggest that these are tectonomagmatic breccias formed when the igneous rocks were still plastic and poorly consolidated. These breccias have been observed mainly within pods of massive sulfides in the southern orebody (Fig. 7A).

4) Nodules of sulfides (Fig. 6D), centimetric in size, form disseminations occurring to the south, external to the orebodies, along an east–west-trending band.

5) Pyrrhotite veinlets (Fig. 6E), with pyrite and minor pentlandite, cross-cut disseminated sulfides.

6) Chalcopyrite veinlets (Fig. 6F) cross-cut disseminated and massive mineralization, and fragments of breccia.

The metal content of the deposit ranges from 0.08 to 7% Ni, 0.1 to 2.5% Cu, 0.01 to 0.09% Co, 0.1 to 0.8 ppm Pd and 0.1 to 0.8 ppm Pt. The highest contents of Ni are located in the core and northern part of the main body (Fig. 7B), in the areas of massive, semimassive and breccia mineralization (see Fig. 7A for comparison). Values higher than 1.2% Ni have been encountered also in disseminated sulfides. Apart from the massive pods, the highest contents of Cu are distributed in the southern and deeper part of the southern body, where disseminated chalcopyrite-rich mineralization is found. The variation of the Ni:Cu ratio with the weight percentage of S in the deposit is shown in Figure 7C.

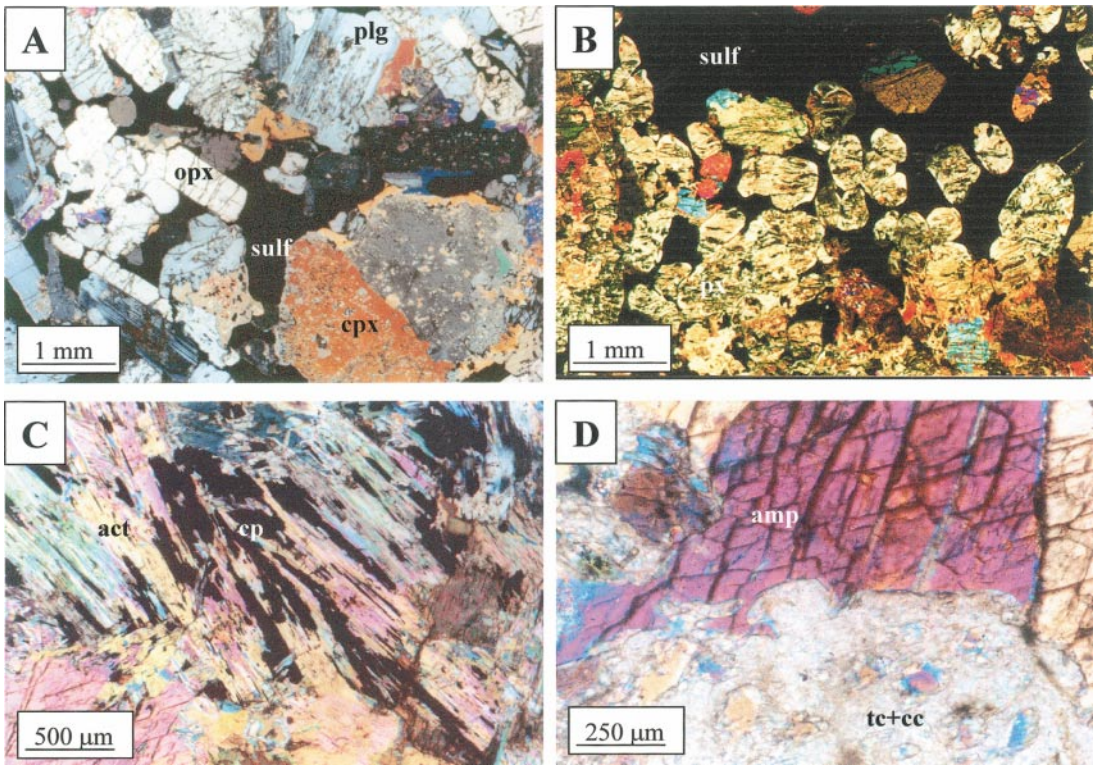

FIG. 5. Sulfide-mineralized igneous rocks. A. Norite with disseminated sulfides (sulf) that occur interstitially to clinopyroxene (cpx), orthopyroxene (opx) and plagioclase (plg). B. Pyroxenite with cumulus pyroxene (px) and massive sulfides (sulf). C. Altered gabbro with tremolite–actinolite (act) extensively replacing clinopyroxene. Chalcopyrite (cp) occurs along cleavage planes of the amphibole. D. Basal section of amphibole (amp) overprinted by a talc–carbonate aggregate (tc+cc). Transmitted light, crossed polars.

Sampling and Analytical Methods

The mineralogy and microtextures of the sulfide ore were investigated in polished samples (both blocks and thin sections) from six drill cores dipping 45°S. Sulfides were studied using reflected-light microscopy and analyzed quantitatively with an electron microprobe. We used a JEOL Superprobe JXA–8900 M instrument, operating at 20 kV and 50 nA at the Centro de Microscopía Electrónica of the Universidad Complutense de Madrid. The PGM were sought in twenty-six polished sections from three drill cores, using scanning electron microscopy and energy-dispersion (EDX) analysis at the School of Earth, Ocean and Planetary Sciences at the University of Cardiff. The scanning electron microscope used is a Cambridge Instruments S360 with a four-quad-

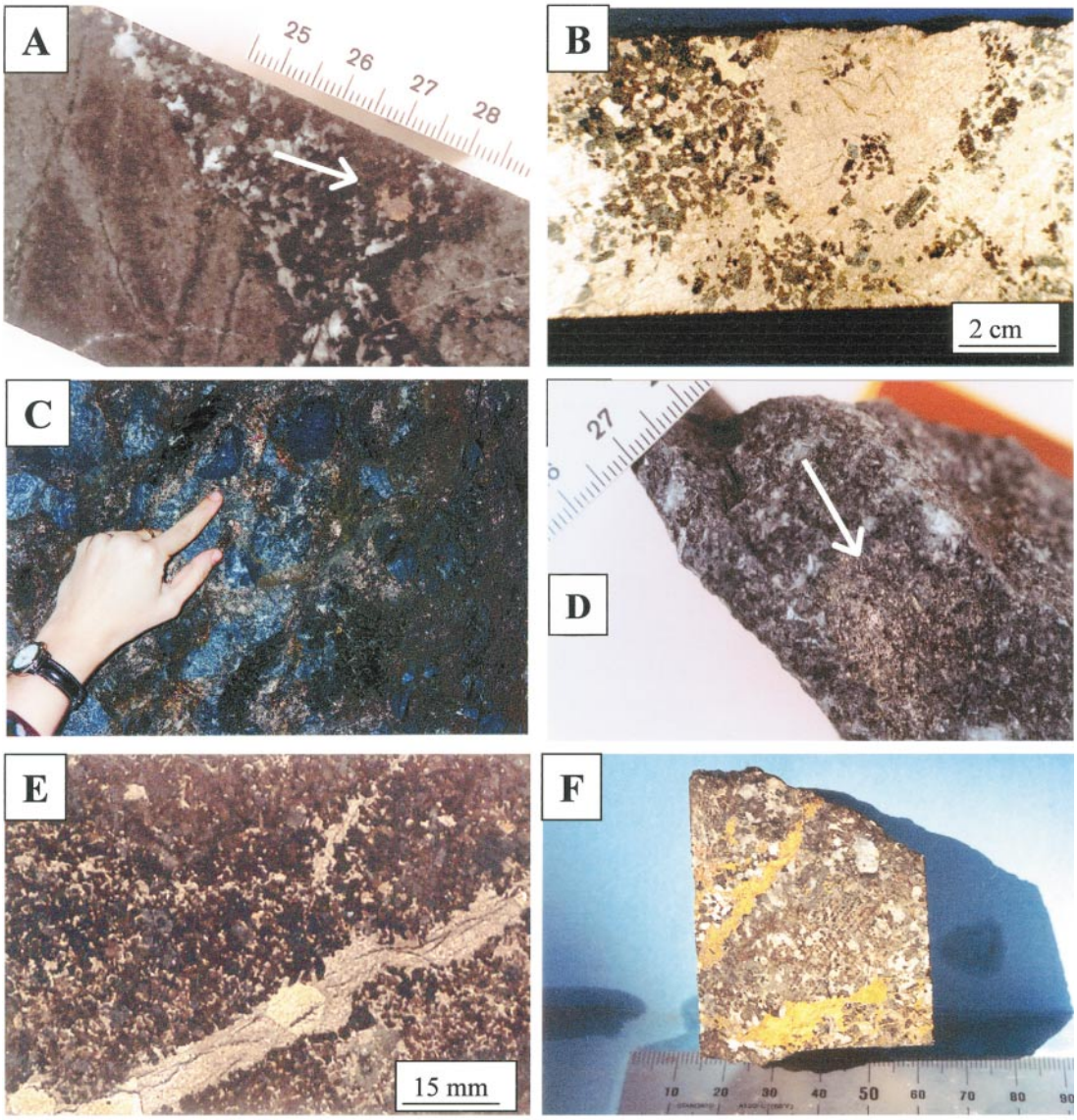

FIG. 6. Types of mineralization. A. Droplets of sulfides disseminated in a leucogabbro hosting fragments of ultramafic rocks. B. Massive sulfides from a drill-core sample. C. Breccia ore exposed in an exploration gallery close to the surface. D. Nodules of sulfides occurring to the south of the southern orebody. E. Disseminated ore cut by a veinlet with pyrrhotite and pyrite. F. Chalcopyrite veinlets in a leucogabbro with disseminated sulfides. Scale bars in centimeters.

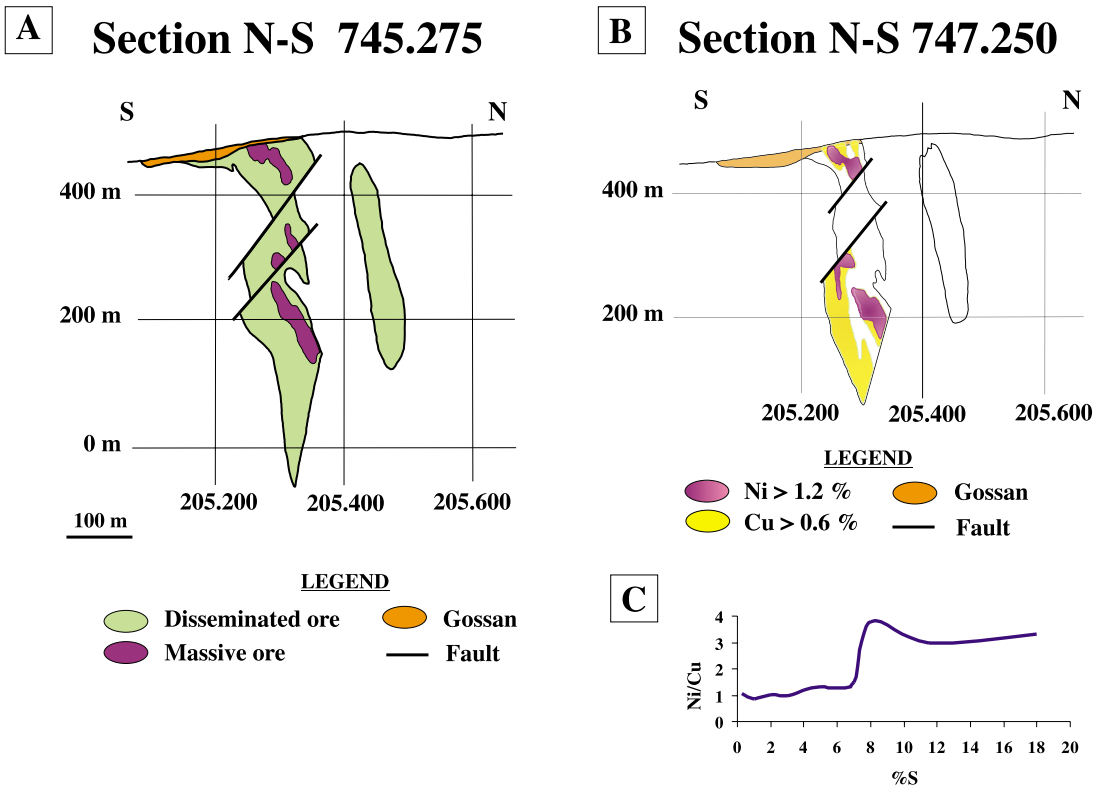

FIG. 7. A. North–south section 745.275 (C–D in Fig. 2) of the orebodies showing the distribution of the massive and disseminated ores. B. North–south section 747.250 (E–F in Fig. 2) showing the distribution of Ni > 1.2 wt% and Cu > 0.6 wt%. C. Ni/Cu *versus* wt% S. Curve calculated using data from 235 representative samples, each of them comprising 2 m of drill core.

rant back-scatter detector (4QBSC) and an Oxford Instruments AN10,000 EDX analyzer, with an accelerating voltage of 20 kV. Selected grains of PGM larger than 5 μm and having a good polished surface were analyzed quantitatively using pure metals as standards.

Eight representative samples in which the PGM were studied using the SEM were chosen for whole-rock analysis for all six PGE, Au and As. These analyses were carried out by Genalysis Laboratory Services Pty. Ltd. (Australia). The precious metals were collected by nickel sulfide fire assay, and the button was analyzed by inductively coupled plasma – mass spectrometry (ICP–MS). Analyses of samples for Au, Pd and Pt were repeated for two samples by lead-collection fire assay using new pots and ICP–MS analysis, and gave similar results to the Ni sulfide fire assay. For the determination of As, the samples underwent multiacid digestion (hydrofluoric, nitric, perchloric and hydrochloric acids) and were analyzed by inductively coupled plasma – optical (atomic) emission spectrometry. All the samples analyzed yielded As contents below the detection limit (5 ppm).

SULFIDE MINERALOGY AND TEXTURES

The Ni–Cu–Fe sulfides consist of pyrrhotite, pentlandite, chalcopyrite and pyrite. Accessory minerals accompanying these major sulfides include magnetite, ilmenite, PGM (sperrylite, michenerite, merenskyite, palladian melonite, irarsite), native gold, tellurobismuthite, hessite, volinskyite, marcasite and violarite.

The sulfide mineralogy is similar in the massive, breccia and disseminated sulfide ores and in the nodules, although there is variation in both the textures and the relative abundances of each sulfide. The massive and breccia ores are characterized by coarse equant anhedral crystals of annealed hexagonal pyrrhotite with sparse exsolution-induced flames of pentlandite, surrounded by polycrystalline, chain-like aggregates of pentlandite (Fig. 8A) and minor chalcopyrite. Magnetite and il-

menite occur as euhedral crystals within the massive sulfides.

The disseminated ore usually contains greater proportions of chalcopyrite than the massive sulfides. Chalcopyrite and pyrrhotite form nodules of millimetric to centimetric size in which the two sulfides are distributed in separate, well-defined domains (Figs. 6A, 8B). This type of texture has been observed in other magmatic Ni–Cu sulfide ores, such as at Noril'sk, where it is interpreted as having been produced by *in situ* fractionation of sulfide droplets (Distler & Kunilov 1994). Pyrrhotite also occurs as irregularly shaped grains surrounded by pentlandite and shows internal twinning as curved lamellae corresponding to a monoclinic polymorph.

The nodules of sulfides occurring to the south of the main orebody consist of irregular grains of pyrrhotite surrounded by coarse pentlandite and anhedral chalcopyrite, the latter being relatively abundant. They usually occur interstitially to the silicates. Several small grains of bismuthite, galena and sulfoarsenides of the cobaltite–gersdorffite series occur within pyrrhotite and pentlandite.

The sulfide assemblage infilling veinlets is of two types. The first type consists of an annealed pyrrhotite and chain-like coarse-grained pentlandite. Veinlets of the second type are filled with massive chalcopyrite with minor pyrrhotite.

The magmatic sulfide assemblage described above is overprinted by hypogene fluid-deposited pyrite, exhibiting a wide variety of textures. It either replaces pyrrhotite or cross-cuts magmatic sulfides and silicates. It can be locally abundant (up to 10% of the sulfides), and occurs notably in areas with strong microfracturing. Textural features, cross-cutting relationships, and Co and Ni content allow the identification of three main generations of pyrite (Fig. 9; Martín Estévez *et al.* 2000):

1) Large euhedral crystals of early pyrite (Py_1) are present throughout the deposit, overprinting the pyrrhotite in all the ore types wherever it is present and observable even in the gabbros and country rocks barren of Ni and Cu sulfides. Py_1 usually occurs in the core of anhedral grains of pyrrhotite, which are surrounded by coarse-grained pentlandite (Fig. 9A). However, in many cases, chain-like pentlandite appears to have nucleated and grown on the faces of the euhedral pyrite (Fig. 9B), thus indicating that this generation of pyrite formed very early in the postmagmatic history of the deposit. Textural evidence of overgrowth and recrystallization of Py_1 crystals has been observed in the pyrrhotite veinlets (Figs. 6E, 9B).

2) Pyrite also forms single crystals or aggregates nucleated on flames of pentlandite within hexagonal pyrrhotite in the massive ore (Py_{2A}, Fig. 9C) and ribbon-like crystals outlining the curved lamellae of monoclinic pyrrhotite in the disseminated ore (Py_{2B}, Fig. 9D). The latter is a rather atypical texture for pyrite, and has been interpreted as the result of preferential nucleation and growth of fluid-deposited pyrite on pre-existing twin planes of the pyrrhotite (Martínez Estévez *et al.* 2000). Py_{2A} and Py_{2B} are commonly accompanied by minor chalcopyrite.

3) Finally, pyrite replaces pyrrhotite as aggregates of small cubic crystals (Py_{3A}, Fig. 9E), replacing plagioclase (Py_{3B}, Fig. 9F) along grain boundaries, and infilling late fractures (Py_{3C}, Fig. 9G).

Postdating the bulk of the pyrite precipitation, an assemblage of supergene sulfides was produced by the alteration of the primary magmatic phases, notably in fractured areas. This assemblage comprises violarite replacing pentlandite along grain boundaries, and marcasite, in some cases as a fine intergrowth with pyrite, replacing pyrrhotite. Only in the uppermost part of the deposit, in the gossan, has an oxidized assemblage been

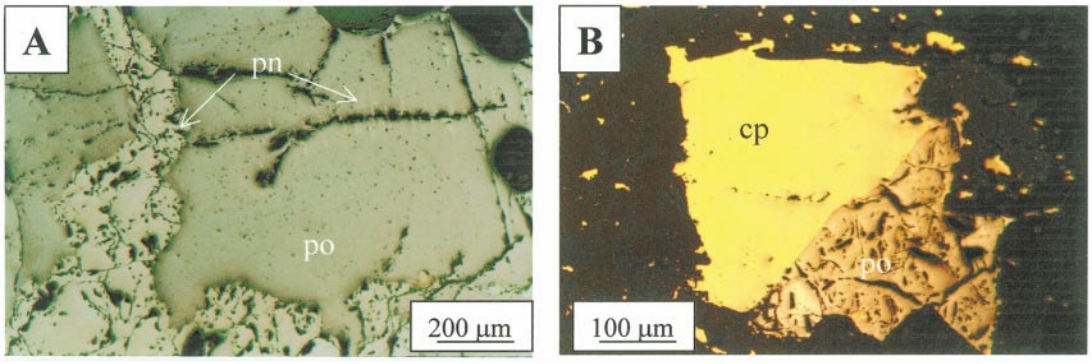

FIG. 8. A. Anhedral pyrrhotite surrounded by chain-like aggregates of pentlandite and containing pentlandite flames. Massive ore. B. A droplet of chalcopyrite and pyrrhotite in the disseminated ore. See text for explanation. Symbols: po: pyrrhotite, pn: pentlandite, cp: chalcopyrite. Reflected light, plane-polarized light, in air.

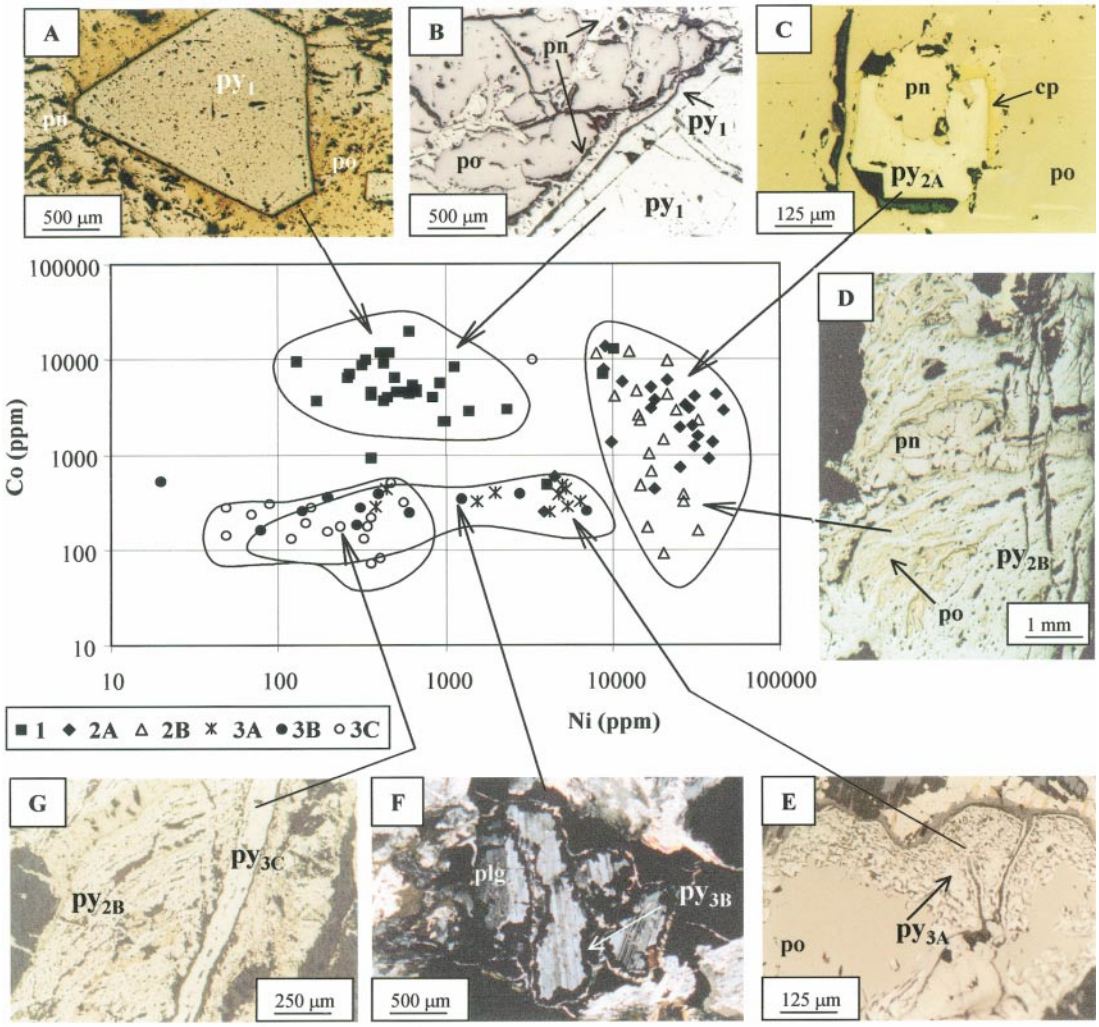

FIG. 9. Textural and geochemical features of pyrite. A. Large euhedral crystal of pyrite (Py_1) overprinting pyrrhotite in the massive ore. B. Detail of a euhedral grain of pyrite (Py_1) in a pyrrhotite veinlet (see Fig. 6E). Subidiomorphic grains of early pyrite are overgrown to form a single large euhedral crystal. C. Pyrite (Py_{2A}) replacing hexagonal pyrrhotite around a rosette of pentlandite. Massive ore. D. Ribbon-like aggregates of pyrite (Py_{2B}) replacing monoclinic pyrrhotite along curved twin lamellae; the remaining pentlandite is unreplaced. E. Mosaic of small subhedral crystals of pyrite (Py_{3A}) replacing pyrrhotite along grain boundaries. F. Pyrite (Py_{3B}) replacing plagioclase at grain boundaries. G. Fractures infilled with pyrite (Py_{3C}), cross-cutting earlier aggregates of ribbon-like pyrite. Symbols: po: pyrrhotite, pn: pentlandite, cp: chalcopyrite, py: pyrite.

developed, formed of garnierite, goethite, malachite and platinum-group oxides.

Results of electron-microprobe analyses (Table 1) show that pyrrhotite interstitial to silicates contains between 59.0 and 60.8 wt.% Fe, with Ni below 0.8 wt.% and traces of Cu (<0.09 wt.%) and Co (<0.1 wt.%). Coarse-grained pentlandite contains between 35.0 and 36.2 wt.% Ni and low Co contents (<0.7 wt%). This composition is in agreement with the assemblage of hexagonal pyrrhotite – monoclinic pyrrhotite – pentlandite of Misra & Fleet (1973). Chalcopyrite has a stoichiometric composition, with only traces of Co. The average metal content in the different textural types of pyrite fits well with the stoichiometric values, and only Py_1 and Py_{2A} contain metal slightly in excess. The main differences between the different types of pyrite are in the Ni and Co contents and Co/Ni values (Fig. 9). The level of Co ranges from 0.02 to 0.45 wt.%, and that of

TABLE 1. REPRESENTATIVE COMPOSITIONS OF MAJOR BASE-METAL SULFIDES, AGUABLANCA Ni–Cu–PGE DEPOSIT, SOUTHWESTERN IBERIA

Anal.	Py type	Ore type	*n*	S	As	Fe	Cu	Co	Ni	Co/Ni	Total	S	As	Fe	Cu	Co	Ni
								Pyrrhotite									
1		D		39.77	n.d.	59.73	n.d.	0.07	0.81		100.38	53.36	n.d.	46.00	n.d.	0.05	0.59
2		D		38.83	n.d.	59.83	n.d.	0.07	0.39		99.12	52.88	n.d.	46.78	n.d.	0.05	0.29
3		D		39.00	n.d.	60.18	0.08	0.06	0.45		99.77	52.80	n.d.	46.77	0.05	0.05	0.33
4		S		40.09	0.04	59.16	0.01	0.07	0.50		99.87	53.89	0.02	45.66	0.01	0.05	0.37
5		S		39.34	n.d.	60.30	0.01	0.06	0.63		100.34	52.92	n.d.	46.56	0.01	0.04	0.47
6		M		38.75	n.d.	59.55	n.d.	0.04	0.65		98.99	52.86	n.d.	46.63	n.d.	0.03	0.48
7		M		39.47	0.1	60.49	0.03	0.07	0.51		101.30	52.93	0.06	46.57	0.02	0.05	0.37
8		M		39.55	n.d.	60.85	0.08	0.09	0.34		100.91	52.91	n.d.	46.73	0.05	0.06	0.25
9		M		39.50	0.05	60.35	0.02	0.09	0.46		100.47	53.05	0.02	46.53	0.01	0.06	0.33
10		M		39.45	0.08	59.73	n.d.	0.09	0.70		100.05	53.18	0.03	46.22	n.d.	0.07	0.50
11		V		38.23	n.d.	60.11	n.d.	0.05	0.75		99.14	52.25	n.d.	47.16	n.d.	0.03	0.56
								Pentlandite									
12		D		33.01	n.d.	29.22	0.01	0.71	35.26		98.21	47.55	n.d.	24.16	0.01	0.55	27.73
13		D		33.61	n.d.	28.68	0.02	0.66	36.17		99.80	47.89	n.d.	23.45	0.01	0.51	28.14
14		D		33.35	0.01	30.74	0.03	0.12	35.09		99.34	47.48	0.01	25.12	0.02	0.09	27.28
								Chalcopyrite									
15		M		34.94	n.d.	31.09	33.51	0.02	n.d.		99.56	50.12	n.d.	25.60	24.26	0.02	n.d.
16		M		34.75	n.d.	31.29	33.50	0.03	n.d.		99.57	49.76	n.d.	25.80	24.42	0.02	n.d.
								Pyrite									
17	Py_1	D	5	52.60	0.02	46.13	n.d.	0.45	0.06	7.5	99.27	66.27	0.01	33.37	n.d.	0.31	0.04
18	Py_{2A}	M	4	52.05	0.01	44.17	0.01	0.11	2.81	0.04	99.15	65.87	0.01	32.09	0.01	0.08	1.94
19	Py_{2B}	D	8	52.32	n.d.	44.63	0.01	0.16	2.14	0.07	99.26	66.06	n.d.	32.34	0.01	0.11	1.48
20	Py_{3A}	M	8	51.44	0.01	46.94	n.d.	0.03	0.32	0.09	98.74	65.46	0.01	34.29	n.d.	0.02	0.22
21	Py_{3B}	S	6	52.11	0.01	46.64	n.d.	0.02	0.12	0.17	98.90	66.99	0.01	33.91	n.d.	0.01	0.08
22	Py_{3C}	M	6	52.77	n.d.	46.53	n.d.	0.02	0.03	0.7	99.34	66.37	n.d.	33.60	n.d.	0.01	0.02

n: number of crystals analyzed. For an explanation of the types of pyrite, see the text. Types of ore: D: disseminated ore, S: semimassive ore, M: massive ore. V: veinlets filled with pyrrhotite. n.d.: not detected.. The compositions are first expressed in wt%, then in atom %.

Ni, from 0.03 to 2.81wt.%, with Co/Ni values below 0.2 in pyrite replacing pyrrhotite ($Py_{2A,B}$ and Py_{3A}) and plagioclase (Py_{3B}), 0.7 for pyrite in late fractures (Py_{3C}), and 7.5 for large crystals of euhedral pyrite (Py_1).

Platinum-Group Minerals

PGM in the sulfide ores

Twenty-six polished sections (3 × 3 cm in size) were examined using the SEM in order to characterize the platinum-group minerals. Of these samples, eight are from the disseminated ore, ten are massive sulfides (including those occurring in the matrix of the breccia ore), three contain massive sulfides with abundant pyrite Py_1, three are of chalcopyrite veinlets, one contains a veinlet with pyrrhotite and pyrite Py_1, and one contains a nodule of sulfides external to the orebodies. Results are displayed in Tables 2 and 3 and Figures 10 to 14. PGM were found to be abundant in these samples, with 217 grains identified. The average number of PGM grains per polished section is variable in the different types of ore: 15 grains per section in the massive ore with large crystals of pyrite Py_1, 10 grains per section in the massive sulfides, five grains per section in the disseminated ore, one grain in the pyrrhotite veinlet, and one grain in the sulfide nodule. In the chalcopyrite veinlets, the number of PGM grains ranges from 5 to 21 per section. These PGM are mostly enclosed in sulfides, notably pyrrhotite (74 grains) and pentlandite (53 grains), although they are generally located close to the edges of the sulfide grains (Figs. 10A, B, C). They also occur in chalcopyrite (39 grains, of which 21 grains are found in a single section of one chalcopyrite veinlet) and in lesser quantities at the contacts between sulfides (12 grains), between sulfides and silicates (19 grains), or enclosed in silicates (17 grains) (Figs. 10D, E, G, H). The PGM are notably absent within pyrite.

The distribution of the PGM by ore types is illustrated in Figure 11, which shows that the occurrence of PGM at the contacts between two minerals is much more common in the disseminated ore and in the massive ore with abundant pyrite Py_1 than in the other ores. The morphology of the PGM varies from euhedral to subhedral and rounded or anhedral. The majority of PGM grains are small, averaging about 4–10 μm and rarely exceeding 15 μm, although exceptionally the PGM are larger, with the largest grain measuring 47 ×

TABLE 2. REPRESENTATIVE COMPOSITIONS OF PLATINUM-GROUP MINERALS, AGUABLANCA Ni–Cu–PGE DEPOSIT, SOUTHWESTERN IBERIA

N°	Ore type	Te	Bi	As	S	Sb	Pd	Pt	Ni	Fe	Cu	Ag	Host
Michenerite													
1[a]	D	38.56	24.23	n.d.	n.d.	3.71	31.44	0.39	0.59	1.01	n.d.	0.27	pn
2[b]	D	35.95	30.68	n.d.	n.d.	n.d.	30.39	n.d.	1.65	1.33	n.d.	n.d.	po/pn
3	D	35.40	26.56	n.d.	n.d.	n.d.	32.44	0.71	2.29	2.60	n.d.	n.d.	pn
4	Mpy	33.87	30.06	n.d	n.d.	1.18	30.64	n.d.	1.62	2.21	n.d.	0.42	p/silicate
Merenskyite													
5	D	54.03	12.82	n.d.	n.d.	n.d.	28.41	n.d.	2.75	1.99	n.d.	n.d.	silicate
6[a]	D	55.79	11.49	n.d.	n.d.	n.d.	26.43	n.d.	5.50	0.79	n.d.	n.d.	pn
7	S	57.29	7.20	n.d.	0.95	n.d.	30.33	n.d.	0.56	3.67	n.d.	n.d.	silicate
8	M	50.21	14.34	n.d.	0.44	n.d.	16.04	10.37	5.61	2.99	n.d.	n.d.	pn
9	Mpy	52.89	17.12	n.d.	n.d.	n.d.	19.99	2.75	7.25	n.d.	n.d.	n.d.	po
10	Mpy	48.33	16.76	n.d.	n.d.	n.d.	20.59	1.86	9.49	2.97	n.d.	n.d.	pn
11	Mpy	45.14	17.74	n.d.	n.d.	0.57	19.89	2.65	9.68	3.57	n.d.	0.76	pn
Moncheite													
12	M	49.46	12.14	n.d.	0.74	n.d.	7.90	15.73	9.41	4.62	n.d.	n.d.	pn
13	M	50.14	16.26	n.d.	n.d.	n.d.	11.03	16.29	3.88	2.40	n.d.	n.d.	po/pn
14	M	50.38	11.79	n.d.	0.61	n.d.	13.22	14.31	4.91	4.78	n.d.	n.d.	po/pn
Palladian melonite													
15	S	58.41	6.07	n.d.	0.66	n.d.	7.65	n.d.	21.47	5.74	n.d.	n.d.	po
16	S	57.5	6.08	n.d.	0.98	n.d.	13.11	n.d.	17.73	4.58	n.d.	n.d.	po
17	S	59.3	5.42	n.d.	0.59	n.d.	9.11	n.d.	21.38	4.19	n.d.	n.d.	po
18	M	58.7	4.64	n.d.	1.02	n.d.	15.66	n.d.	16.93	3.09	n.d.	n.d.	pn
Sperrylite													
19	D	n.d.	n.d.	63.66	1.65	n.d.	n.d.	34.01	n.d.	0.52	0.16	n.d.	silicate
20	M	n.d.	n.d.	59.04	1.41	n.d.	n.d.	31.72	n.d.	4.13	3.70	n.d.	cp
21	Mpy	n.d.	n.d.	64.72	0.77	n.d.	n.d.	33.48	n.d.	1.03	n.d.	n.d.	silicate

N°	Ore type	Te	Bi	As	S	Sb	Pd	Pt	Ni	Fe	Cu	Ag	Host
Michenerite													
1[a]	D	38.56	24.23	n.d.	n.d.	3.71	31.44	0.39	0.59	1.01	n.d.	0.27	pn
2[b]	D	35.95	30.68	n.d.	n.d.	n.d.	30.39	n.d.	1.65	1.33	n.d.	n.d.	po/pn
3	D	35.40	26.56	n.d.	n.d.	n.d.	32.44	0.71	2.29	2.60	n.d.	n.d.	pn
4	Mpy	33.87	30.06	n.d	n.d.	1.18	30.64	n.d.	1.62	2.21	n.d.	0.42	p/silicate
Merenskyite													
5	D	54.03	12.82	n.d.	n.d.	n.d.	28.41	n.d.	2.75	1.99	n.d.	n.d.	silicate
6[a]	D	55.79	11.49	n.d.	n.d.	n.d.	26.43	n.d.	5.50	0.79	n.d.	n.d.	pn
7	S	57.29	7.20	n.d.	0.95	n.d.	30.33	n.d.	0.56	3.67	n.d.	n.d.	silicate
8	M	50.21	14.34	n.d.	0.44	n.d.	16.04	10.37	5.61	2.99	n.d.	n.d.	pn
9	Mpy	52.89	17.12	n.d.	n.d.	n.d.	19.99	2.75	7.25	n.d.	n.d.	n.d.	po
10	Mpy	48.33	16.76	n.d.	n.d.	n.d.	20.59	1.86	9.49	2.97	n.d.	n.d.	pn
11	Mpy	45.14	17.74	n.d.	n.d.	0.57	19.89	2.65	9.68	3.57	n.d.	0.76	pn
Moncheite													
12	M	49.46	12.14	n.d.	0.74	n.d.	7.90	15.73	9.41	4.62	n.d.	n.d.	pn
13	M	50.14	16.26	n.d.	n.d.	n.d.	11.03	16.29	3.88	2.40	n.d.	n.d.	po/pn
14	M	50.38	11.79	n.d.	0.61	n.d.	13.22	14.31	4.91	4.78	n.d.	n.d.	po/pn
Palladian melonite													
15	S	58.41	6.07	n.d.	0.66	n.d.	7.65	n.d.	21.47	5.74	n.d.	n.d.	po
16	S	57.5	6.08	n.d.	0.98	n.d.	13.11	n.d.	17.73	4.58	n.d.	n.d.	po
17	S	59.3	5.42	n.d.	0.59	n.d.	9.11	n.d.	21.38	4.19	n.d.	n.d.	po
18	M	58.7	4.64	n.d.	1.02	n.d.	15.66	n.d.	16.93	3.09	n.d.	n.d.	pn
Sperrylite													
19	D	n.d.	n.d.	63.66	1.65	n.d.	n.d.	34.01	n.d.	0.52	0.16	n.d.	silicate
20	M	n.d.	n.d.	59.04	1.41	n.d.	n.d.	31.72	n.d.	4.13	3.70	n.d.	cp
21	Mpy	n.d.	n.d.	64.72	0.77	n.d.	n.d.	33.48	n.d.	1.03	n.d.	n.d.	silicate

Compositions are reported in wt. % on the left, and in atom % on the right. a: Composite grain with merenskyite and michenerite. b: Composite grain with michenerite, hessite and volynskite (Table 3, anal. 4 and 5). n.d.: not detected. D: disseminated ore, S: semimassive ore, M: massive ore, Mpy: massive ore with abundant pyrite. Symbols: pn: pentlandite, po: pyrrhotite, cp: chalcopyrite, po/pn: at the contact between pyrrhotite and pentlandite.

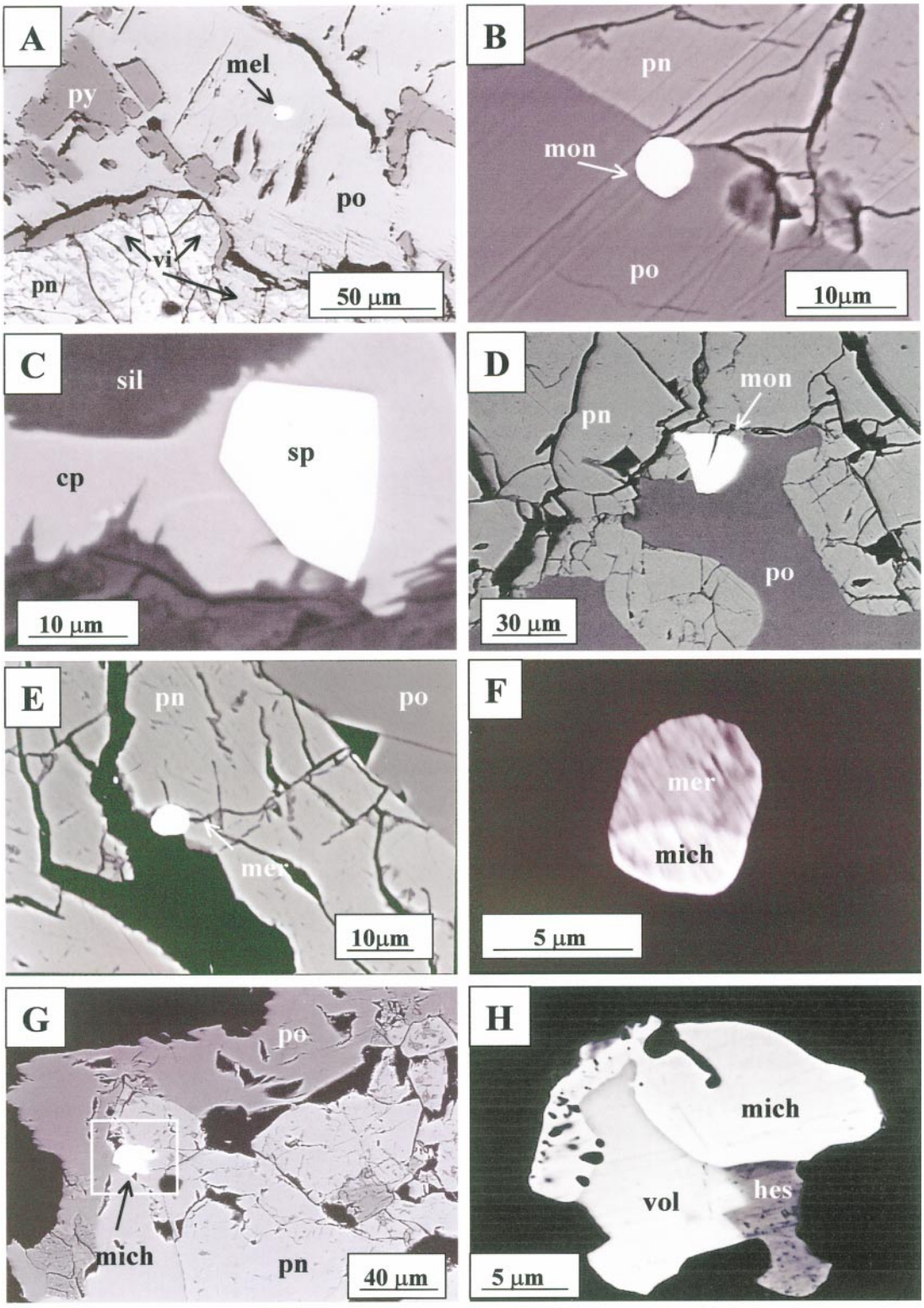
A
mel
py
po
vi
pn
50 μm
B
pn
mon
po
10μm
C
sil
sp
cp
10 μm
D
mon
pn
po
30 μm
E
pn
po
mer
10μm
F
mer
mich
5 μm
G
po
mich
pn
40 μm
H
mich
vol
hes
5 μm

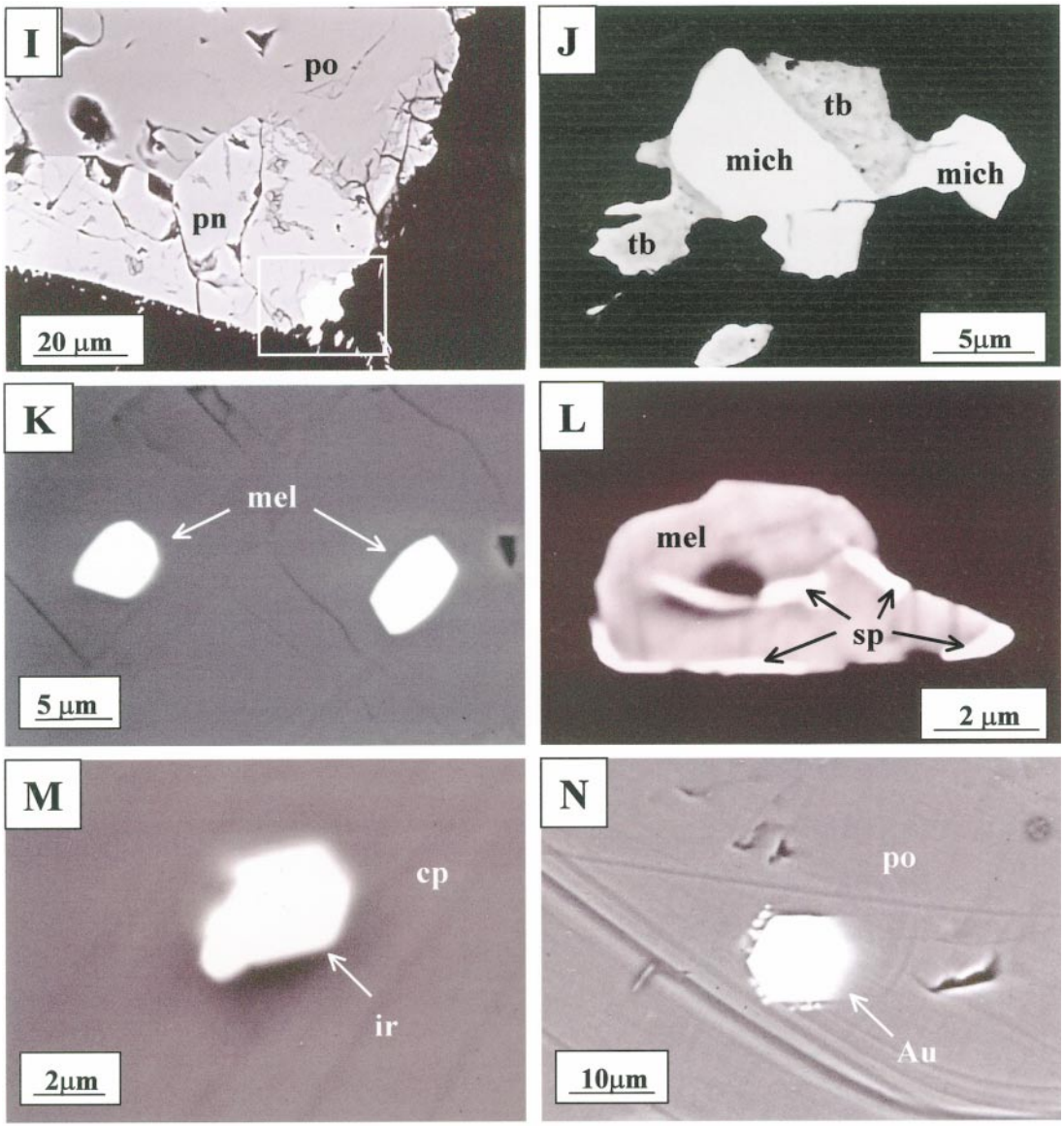

FIG. 10. Back-scattered electron images of platinum-group minerals. A. Melonite within pyrrhotite in the massive ore. B. Subhedral moncheite in pyrrhotite in contact with pentlandite, massive ore. C. Subhedral sperrylite within chalcopyrite in the disseminated ore. D. Irregularly shaped moncheite at the contact between pyrrhotite and pentlandite. E. Pt-bearing merenskyite at the edge of pentlandite, massive ore. F. A composite grain of Pt-free merenskyite and michenerite within pyrrhotite, massive ore. G. A composite grain of michenerite and tellurides in pentlandite at the contact with pyrrhotite. H. Detail of this composite grain containing michenerite, volynskite and hessite. I. A composite PGM grain at the edge of pentlandite. J. Detail of the composite grain, containing michenerite and tellurobismuthite. K. Subhedral grains of palladian melonite within pyrrhotite, semimassive ore. L. Composite grain of palladian melonite with elongate grains of sperrylite, semimassive ore. M. Subhedral irarsite (?) in chalcopyrite, disseminated ore. N. Euhedral crystal of gold within pyrrhotite close to the contact with chalcopyrite, massive ore. Symbols: po: pyrrhotite, pn: pentlandite, cp: chalcopyrite, py: pyrite, sil: silicates, mel: melonite, mon: moncheite, mer: merenskyite, mich: michenerite, sp: sperrylite, ir: irarsite, Au: gold, vol: volynskite, hes: hessite, tb: tellurobismuthite.

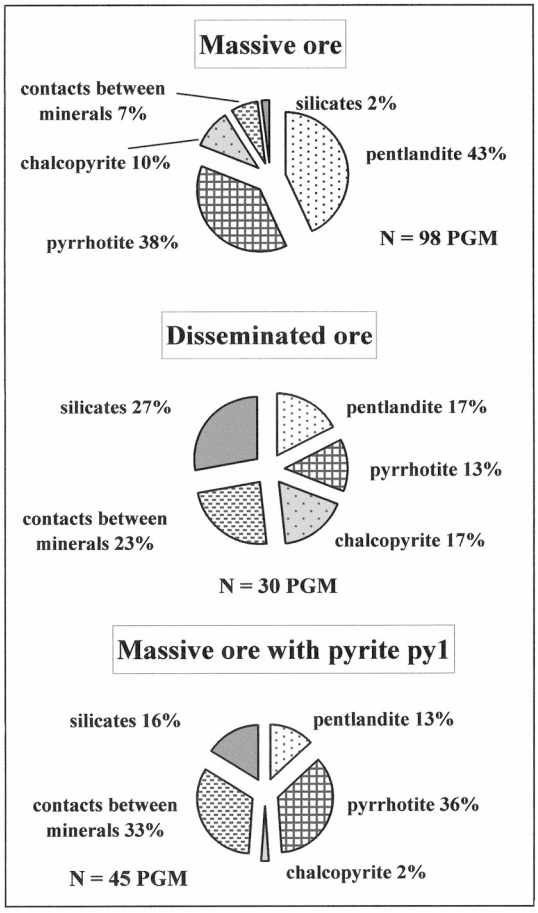

FIG. 11. Distribution of platinum-group minerals in their host minerals in the massive ore without pyrite, in the disseminated ore and in the massive ore with abundant Py_1 pyrite.

35 μm. The small size of the PGM grains severely limits quantitative determinations. Nevertheless, quantitative analyses were obtained for the larger grains, which allowed the identification of several types of PGM (Table 2). Traces of S, Fe and Cu detected in many PGM may indicate some contamination from the host sulfides owing to the size of the grains.

Although some arsenides and sulfarsenides such as sperrylite ($PtAs_2$) and Ir–Os–As–S-bearing phases are found in the Aguablanca suite, Pt and Pd tellurides and bismuthotellurides are dominant. These PGM comprise michenerite, merenskyite, palladian bismuthian melonite and moncheite. The Pd tellurides (michenerite, palladian melonite and some of the merenskyite) are more abundant (117 grains) than those containing both Pd and Pt (61 grains of moncheite and Pt-bearing merenskyite). The nodule of sulfides and the pyrrhotite veinlet both contain only one grain of michenerite. Most of the PGM occur as single grains, although the presence of composite grains is common. These are composed of two or three phases of similar composition, mostly michenerite + merenskyite and michenerite + non-PGE tellurides. The latter include bismuth-, bismuth–silver- and silver-bearing tellurides such as tellurobismuthite (Bi_2Te_3), volynskite ($AgBiTe_2$) and hessite (Ag_2Te), which occur both associated with PGM and as individual grains. Two grains of native gold also were found spatially related to the PGM.

Michenerite is ubiquitous and abundant throughout the deposit; it occurs as grains with rounded boundaries and with irregular to elongate shapes. It is usually less than 15 μm in size. The michenerite analyzed (Table 2) shows Pt and Ag substituting for Pd, whereas Sb may substitute for Bi. The presence of Ni and Fe may result either from substitution for Pd or from slight contamination from the host during analysis, owing to the small size of the grains. Michenerite usually forms individual crystals; however, it may occur as part of composite grains (Figs. 10F to 10J). Two examples are included in Table 2. In the first case, the composite grain consists of michenerite of composition $(Pd_{0.89}Pt_{0.01}Fe_{0.03}Ni_{0.17}Ag_{0.01})_{\Sigma 1.11}$ $(Bi_{0.68}Sb_{0.11})$ $Te_{1.10}$ and merenskyite with

TABLE 3. REPRESENTATIVE COMPOSITIONS OF TELLURIDES AND NATIVE GOLD ASSOCIATED WITH PGM, AGUABLANCA Ni–Cu–PGE DEPOSIT, SOUTHWESTERN IBERIA

Anal.		Te	Bi	Sb	Ag	Au	Fe	Ni	Total	Te	Bi	Sb	Ag	Au	Fe	Ni
1	tb	47.64	51.82	n.d.	n.d.	n.d.	n.d.	n.d.	99.46	60.09	39.91	n.d.	n.d.	n.d.	n.d.	n.d.
2	gold	n.d.	n.d.	n.d.	11.44	85.86	1.43	n.d.	98.73	n.d.	n.d.	n.d.	18.69	76.81	4.5	n.d.
3[a]	hes	38.21	n.d.	n.d.	61.17	n.d.	n.d.	n.d.	99.38	34.56	n.d.	n.d.	65.44	n.d.	n.d.	n.d.
4[a]	vol	44.66	36.21	0.18	18.04	n.d.	0.79	0.12	100.00	49.43	24.47	0.21	23.62	n.d.	1.99	0.28
5[b]	tb	47.15	51.55	n.d.	n.d.	n.d.	0.82	n.d.	99.52	58.57	39.09	n.d.	n.d.	n.d.	2.34	n.d.
6[b]	hes	39.06	n.d.	n.d.	60.57	n.d.	n.d.	n.d.	99.63	35.28	n.d.	n.d.	64.72	n.d.	n.d.	n.d.

Compositions are reported in wt. % on the left, and in atom % on the right. a: Composite grain with tellurobismuthite (tb) and hessite (hes). b: Composite grain with michenerite (see Table 2, anal. 2), hessite and volynskite (vol).

the formula $(Pd_{0.80}Fe_{0.02}Ni_{0.16})_{\Sigma 0.98}$ $Bi_{0.34}$ $Te_{1.68}$ (anal. 1 and 6, Table 2). This grain is hosted by pentlandite in disseminated ore. A composite grain of this type is illustrated in Figure 10F and exemplifies the existence of a partial solid-solution series between merenskyite and michenerite observed in other deposits (*e.g.*, Harney & Merkle 1990). In the second example (Figs. 10G, H), an irregularly shaped grain of michenerite [$(Pd_{0.91}Fe_{0.04}Ni_{0.05})_{\Sigma 1}$ $Bi_{0.92}$ $Te_{1.08}$, anal. 2 in Table 2] occurs with hessite ($Ag_{1.96}Te_{1.04}$) and volynskite [$Ag_{0.94}Fe_{0.08}Ni_{0.01}$ ($Bi_{0.99}$ $Sb_{0.01}$) $Te_{1.97}$] (anal. 4 and 5, Table 3) at the contact between pentlandite and pyrrhotite in the disseminated ore.

Merenskyite is also a very abundant PGE telluride at Aguablanca and exhibits variations in its composition. Many grains consist of Pt-free merenskyite, with Ni up to 2.6 wt.% (anal. 5, 6, and 7 in Table 2; Fig. 12). However, intermediate members of the solid-solution series merenskyite–moncheite ($PdTe_2$–$PtTe_2$, Daltry & Wilson 1997, Cabri 2002) are very common (anal. from 9 to 14 in Table 2; Figs. 10C, D, and 12). They account for up to 36% of the PGM grains found in the massive ore, being less abundant (16%) in the disseminated ore, and they have not been found in the chalcopyrite veinlets. It is noteworthy that phases with a composition close to the $PtTe_2$ end-member have not been observed so far. Both merenskyite and moncheite occur as subhedral to subrounded grains, in some cases anhedral, usually less than 10 μm across (Figs. 10B, D, and E). However, some large grains up to 35 × 25 μm have been observed. In these PGM, extensive substitution of Bi for Te increases from Pt-free merenskyite [*e.g.*, $(Pd_{0.90}Fe_{0.11}Ni_{0.02})_{\Sigma 1.03}$ $Bi_{0.22}$ $Te_{1.72}S_{0.03}$, anal. 7 in Table 2] to Pt-bearing phases (merenskyite–moncheite) [*e.g.*, $(Pd_{0.33}Pt_{0.49}Fe_{0.07}Ni_{0.12})_{\Sigma 1.01}$ $Bi_{0.49}Te_{1.5}$, anal. 13 in Table 2]. According to the experimental results in the system Pd–Bi–Te (Hoffman & MacLean 1976, Makovicky 2002), the compositional data on merenskyite from Aguablanca indicate closure temperatures below 500°C (Fig. 13).

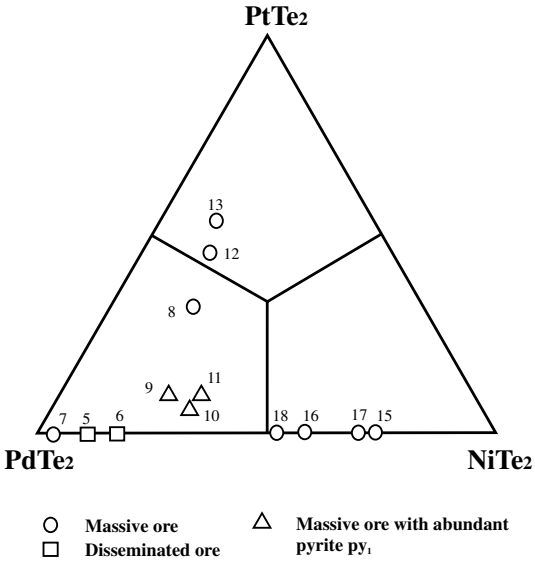

FIG. 12. Chemical composition of the tellurides at Aguablanca in terms of the diagram $PtTe_2$–$PdTe_2$–$NiTe_2$. Numbers refer to compositions in Table 2.

In addition to the substitution involving Pt and Pd, merenskyite and moncheite also exhibit substitution of Ni for Pd (Fig. 12), with maximum values for Pt-bearing merenskyite (up to 4.4 wt.%; anal. 11 in Table 2). Pt-free merenskyite usually occurs as isolated grains, but in composite grains, it is invariably associated with michenerite. In contrast, Pt-bearing merenskyite and moncheite do not form composite grains, and only one small grain (4.6 × 2 μm) shows two zones with different Bi contents. However, whether this corresponds to two separate phases is difficult to ascertain owing to the small size of the grain.

Merenskyite also forms a solid-solution series with melonite ($NiTe_2$) (Cabri 1981, 2002, Daltry & Wilson 1997), and part of this series is found in Aguablanca as palladian bismuthian melonite (Table 2, Fig. 12). The melonite at Aguablanca occurs as small (usually less than 5 μm) subhedral crystals in the unaltered massive ore, enclosed either in pyrrhotite or in pentlandite (Figs. 10A, K). As in the other PGM, substitution of Bi for Te is also observed in melonite, although to a lesser extent. The pure end-member of melonite, $NiTe_2$, has not been found, and Pd is replaced by Ni over the range from $(Ni_{0.65}Pd_{0.23}Fe_{0.17})_{\Sigma 1.05}$ $Bi_{0.18}Te_{1.77}$ to $(Ni_{0.50}Pd_{0.47}Fe_{0.10})_{\Sigma 1.07}$ $Bi_{0.14}Te_{1.76}S_{0.03}$ (anal. 15 and 18 in Table 2), close to the compositional field of merenskyite. No traces of Pt have been detected in melonite. However, in two grains of melonite, tiny inclusions of sperrylite were observed. Melonite occasionally occurs in composite grains with tellurobismuthite or with michenerite.

Sperrylite is not abundant in these samples (only 5% of the total identified PGM grains), but it usually occurs as euhedral grains that are larger than the other PGM (15–30 μm, Fig. 10E). The grains are usually enclosed in sulfides, mostly chalcopyrite, although they also occur within pyroxene, and have been found in both the massive and the disseminated ores. Large crystals of sperrylite are very homogeneous [*e.g.*, $(Pt_{1.02}Fe_{0.02})_{\Sigma 1.04}$ $As_{1.91}S_{0.05}$, anal. 19 in Table 2], and do not form composite grains; only one example has been found, included in melonite.

Apart from the major Pd- and Pt-bearing PGM, minor phases containing Os–Ir–As–S (two grains), Ir–As–S (three grains) and Ir–Pt–As (13 grains) have been located, but are too small for quantitative analysis. The two former grains could be irarsite (Fig. 10M), whereas the latter possibly correspond to an unidentified PGM phase first reported by Stumpfl (1961), with the com-

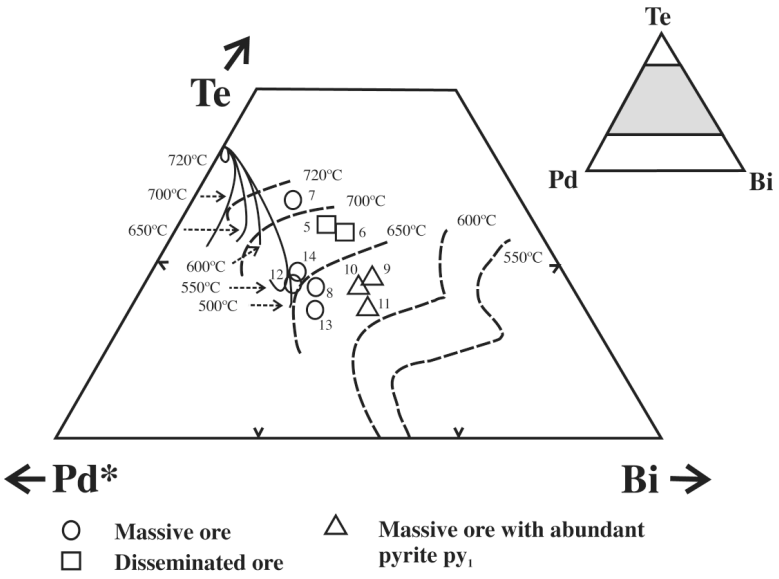

FIG. 13. Plot of tellurides at Aguablanca in the system Pd–Te–Bi. Solid lines correspond to the composition of merenskyite at different temperatures, whereas the dashed lines represent compositions of the coexisting liquid. After Hoffman & MacLean (1976). Pd* = Pd + Pt + Fe + Ni. Numbers refer to compositions in Table 2.

position (Pt,Ir)As_2. The Os–Ir–As–S phase occurs as two rounded grains (the larger is 2.2 × 1.3 μm) enclosed in chalcopyrite from the disseminated ore in the deeper and southernmost part of the main mineralized body. All the grains of the Ir–As–S and the Ir–Pt–As phases (the largest is 1.9 × 1.9 μm) were found in a single veinlet of chalcopyrite cross-cutting the massive ore. The Ir sulfarsenides form groups and clusters within chalcopyrite, whereas the Pt-bearing arsenides are situated in pyrrhotite within the chalcopyrite vein.

Two grains of native gold have been found in this study. One of them is an idiomorphic crystal (9 × 9.6 μm, Fig. 10N) with the formula $Au_{0.77}$ $Ag_{0.18}$ $Fe_{0.05}$ (anal. 6 in Table 3). It occurs in the massive ore within a pyrrhotite grain with patches of chalcopyrite, very close to the contact with plagioclase. The second grain with rounded edges (5 × 6 μm) was also found in pyrrhotite from the massive ore, very close to a veinlet of chalcopyrite. No quantitative analysis was obtained for this grain, but Ag and traces of Fe were detected.

PGE oxides in the gossan

Five samples of gossan from the Aguablanca deposit have been examined for PGM and found to contain Pd bismuthotellurides and sperrylite ranging from 5 to 30 μm in diameter, mimicking the mode of occurrence of the primary PGM. Other associated PGM are oxides, possibly including hydroxides, as indicated by quantitative analyses (Table 4). These oxides either surround the Pd bismuthotellurides and sperrylite, form in patches within them or, in some cases, completely replace them, producing a pseudomorph of the precursor PGM. Pd–Pt–Cu–Fe oxides (anal. 1 and 2, Table 4) occur as mottled and zoned minerals with a euhedral outline, probably representing the boundaries of the original PGM surrounded by magnetite (Fig. 14A). A Pd–Cu oxide (anal. 3 and 4, Table 4) replaces Pd bismuthotellurides, producing a mottled texture (Figs. 14B, C) in a pseudomorph surrounded by Cu oxide. A zoned Pt–Fe oxide (anal. 5 and 6, Table 4) has a euhedral shape, is over 40 × 20 μm in size, and is located with hematite (Figs. 14D, E).

Compositions 1–4, calculated as oxides, have totals approaching 100%, whereas compositions 5 and 6 have low totals. It is possible that these latter pertain to Pt–Fe hydroxides. Low totals cannot be due to the small size of the grains, which are relatively large (40 × 20 μm). These PGM oxides and hydroxides contain traces of SiO_2 and Al_2O_3, which may have been introduced into their structure during alteration of the earlier-formed PGM. Traces of Te and Bi may be remnants from the original PGM from which these minerals formed.

Distribution of Platinum-Group Elements

Eight representative whole-rock samples with a known distribution of PGM were selected for the determination of their PGE content (Table 5). It is generally assumed that the PGE concentrate within the sulfides, as a sulfide melt plays a dominant role as a collector of PGE in mafic–ultramafic magmas (Naldrett & Duke 1980, Barnes *et al.* 1997, Naldrett 1999, Farrow & Lightfoot 2002). This association also is observed in Aguablanca, where the mineralogical study of the ore has shown that PGM are mostly located within the sulfides. Therefore, the PGE contents in the analyzed samples have been recalculated to 100% sulfides and normalized to chondrite. Results are displayed in Figure 15.

The chondrite-normalized PGE diagrams show a general positive slope, with low Os, Ir, Ru and Rh, a negative anomaly in Ru, and some peaks in Pt and Pd. This profile reflects the observed PGM mineralogy. In the case of Au, the distribution is erratic. The highest PGE contents are found in the sulfide fraction of the disseminated ore, which is notably enriched in Pt and Pd with respect to the other ores. This enrichment is extreme in the disseminated sulfides (anal. 2 in Table 5) from the Cu-rich area occurring in the southern and deepest part of the southern orebody (Fig. 7B). The chondrite-normalized PGE diagram for the massive ore (anal. 3, Table 5) displays a kinked pattern, resulting from negative anomalies in Ru and Pt. The negative Pt anomaly is not in agreement with the observed PGM in this and other samples of massive ore, which contain abundant Pt-bearing tellurides. The massive sulfides containing an overprint of abundant py_1-type pyrite (anal. 4 in Table 5) have a more marked enrichment in Pd and Pt.

The (Pt + Pd) : (Ru + Ir + Os) ratio varies among the ore types. The Cu-rich disseminated ore along the southern border of the deposit (anal. 2, Table 5) shows a ratio of 30.7, nine times the value of the other disseminated sulfides (anal. 1, Table 5) and up to fifteen times the value for the pyrite-poor massive ore (anal. 3, Table 5). This Cu-rich ore consists of chalcopyrite, pyrrhotite and pentlandite interstitial to the silicates, together displaying magmatic textures. These features strongly suggest that the preferential concentration of Pd and Pt in the Cu-rich ore is a primary magmatic feature. The massive sulfides overprinted by abundant pyrite py_1 (anal. 4, Table 5) have a (Pt + Pd) : (Ru + Ir + Os) ratio between that in the fractionated disseminated ore and that in the unaltered massive ore. This ratio is unlikely to be a magmatic feature, but rather it may reflect some postmagmatic mobilization of Pd and Pt in certain localized areas. Such mobilization is indicated also by the much higher proportion of PGM located at the contacts between minerals, rather than enclosed within them, as compared with those in the unaltered massive ore.

The two samples of chalcopyrite veinlets analyzed have PGE patterns that are different from each other and that broadly mimic the patterns in the ores that they cut. In this sense, the veinlet that crosses the disseminated ore at the southern border of the main orebody (anal. 6 in Table 5, Fig. 15) has an extreme enrichment in Pd, resembling the Pd concentration observed in this area (anal. 2 in Table 5, Fig. 15). In contrast, the other veinlet of chalcopyrite (anal. 5 in Table 5, Fig. 15) has a pattern similar to that in the massive sulfides that it cross-cuts (anal. 3 in Table 5, Fig. 15), with the exception of a negative Pd anomaly and a dissimilar Au content. The chalcopyrite veinlet cross-cutting the Cu-rich disseminated ore also displays a high (Pt + Pd) : (Ru + Ir + Os) ratio, 48.4, almost fifteen times the ratio in the chalcopyrite veinlet cross-cutting the massive ore (anal. 6 and 5, respectively, Table 5).

The nodules of sulfides display a positive PGE trend, with progressively increasing values for Pt, Pd and Au, respectively, as expected from the PGM observed in this type of mineralization.

TABLE 4. COMPOSITIONS OF PGE OXIDES FROM GOSSANS, AGUABLANCA Ni–Cu–PGE DEPOSIT, SOUTHWESTERN IBERIA

	LO5-B1 1	LO5-C1A 2	LO2-B12A 3	LO2-B12B 4	LO4-A1A 5	LO4-A1B 6
PtO wt%	16.5	13.3	n.d.	n.d.	36.0	27.7
PdO	32.7	46.8	38.0	38.7	2.5	2.1
CuO	10.4	16.6	50.8	45.4	1.3	1.3
MnO	1.0	0.8	n.d.	n.d.	n.d.	n.d.
SiO_2	2.3	1.1	2.3	2.2	2.1	3.0
TeO_2	1.0	n.d.	1	3.2	n.d.	n.d.
Fe_2O_3	35.6	20.0	2.5	2.4	34.6	46.6
Al_2O_3	0.6	n.d.	n.d.	n.d.	0.9	1.4
NiO	n.d.	0.4	1.2	1.4	0.8	0.8
SO_3	n.d.	0.8	1.7	1.7	n.d.	n.d.
Bi_2O_3	n.d.	1.1	n.d.	3.1	n.d.	n.d.
CaO	n.d.	n.d.	n.d.	n.d.	0.4	0.3
As_2O_3	n.d.	n.d.	n.d.	n.d.	n.d.	n.d.
Total	100.1	100.9	97.5	98.1	78.6	83.2

TABLE 5. LEVELS OF PLATINUM-GROUP ELEMENTS IN REPRESENTATIVE WHOLE-ROCK SAMPLES, AGUABLANCA Ni–Cu–PGE DEPOSIT, SOUTHWESTERN IBERIA

N°	Ore type	Os	Ir	Ru	Rh	Pt	Pd	Au	(Pt+Pd)/(Ru+Ir+Os)
1	Disseminated	36	54	54	30	320	155	90	3.30
2	Disseminated	26	64	28	56	2900	720	295	30.68
3	Massive	140	285	155	220	460	720	15	2.03
4	Massive with Py_1	30	62	36	62	1040	1060	50	16.41
5	Cp veinlet	66	136	93	122	662	331	1805	3.36
6	Cp veinlet	13	25	17	28	150	2513	262	48.42
7	Sulfide nodule	3	6	7	6	152	55	30	12.90
8	Sulfide nodule	3	4	5	4	89	53	26	11.83

Concentrations are reported in ppb.

Discussion and Conclusions: Genesis and Retrograde Evolution of the Deposit

The structural, mineralogical, textural and geochemical features described above suggest that the Aguablanca Ni–Cu–PGE ore is the result of a complex evolution due to at least two major events: 1) magmatic crystallization and subsolidus re-equilibration of a sulfide-rich immiscible melt or melts coexisting with a mafic–ultramafic silicate magma, and 2) circulation of hydrothermal fluids related to the development of skarns in the carbonate host-rocks. In the following discussion of these events, we will consider magmatic crystallization of rocks and ores, and then the different processes that took place during the postmagmatic evolution of the deposit.

The magmatic stage

Massive ore is enriched in Ni, whereas the Ni content of disseminated ore is rather heterogeneous, with no apparent relationship with the type of host rock. The disseminated mineralization occurring in the southernmost and deepest part of the deposit is characterized by Cu and PGE contents (in 100% sulfides) higher than in other areas with disseminated sulfides (Figs. 7A, B, 15). In addition, the (Pt + Pd)/(Ru + Ir + Os) value is also higher at the southern margin of the ore (Table 5), up to

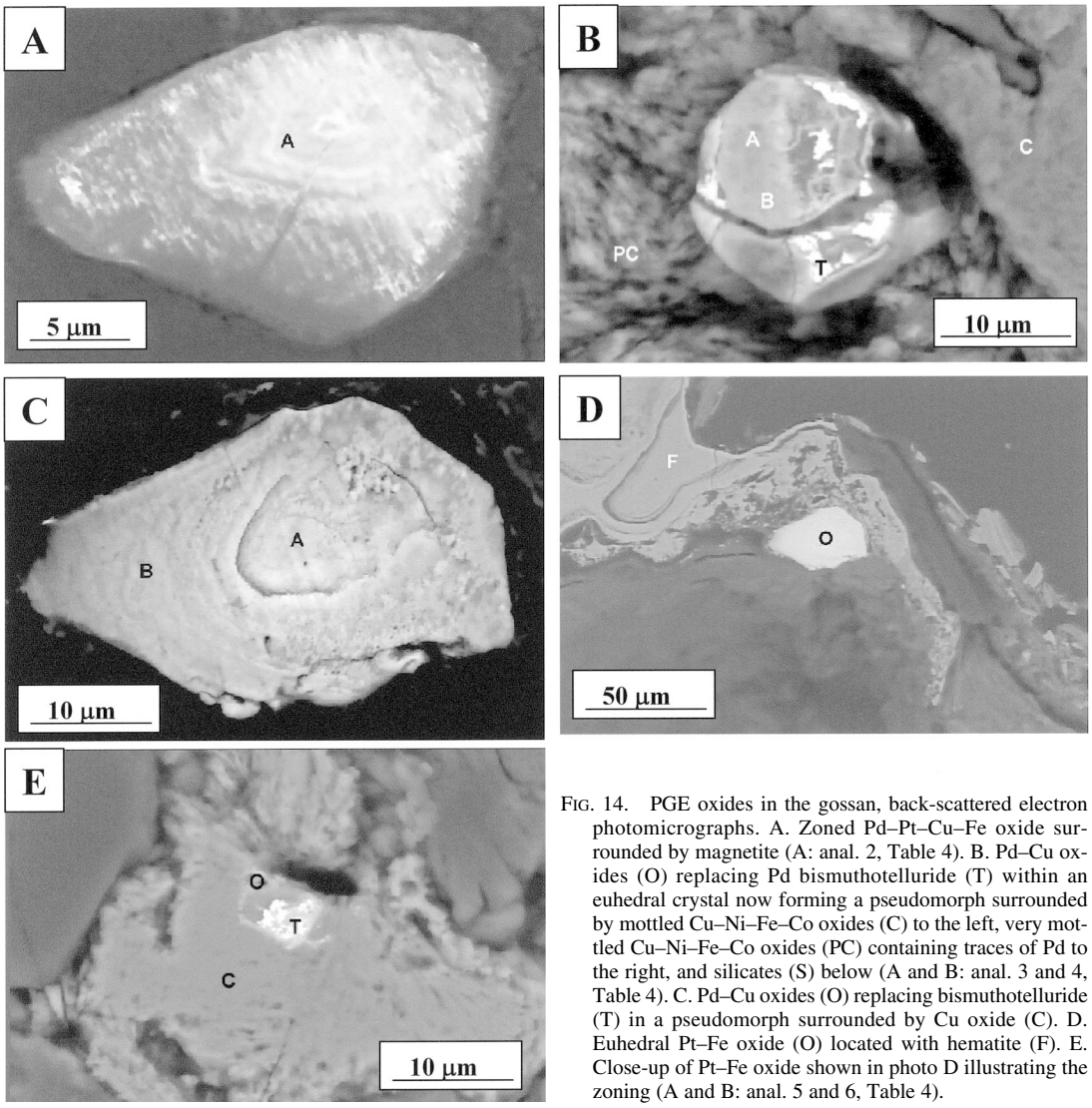

Fig. 14. PGE oxides in the gossan, back-scattered electron photomicrographs. A. Zoned Pd–Pt–Cu–Fe oxide surrounded by magnetite (A: anal. 2, Table 4). B. Pd–Cu oxides (O) replacing Pd bismuthotelluride (T) within an euhedral crystal now forming a pseudomorph surrounded by mottled Cu–Ni–Fe–Co oxides (C) to the left, very mottled Cu–Ni–Fe–Co oxides (PC) containing traces of Pd to the right, and silicates (S) below (A and B: anal. 3 and 4, Table 4). C. Pd–Cu oxides (O) replacing bismuthotelluride (T) in a pseudomorph surrounded by Cu oxide (C). D. Euhedral Pt–Fe oxide (O) located with hematite (F). E. Close-up of Pt–Fe oxide shown in photo D illustrating the zoning (A and B: anal. 5 and 6, Table 4).

nine times the value of the disseminated sulfides in the northern mineralized body. Compared to the massive ore, this Cu-rich disseminated mineralization is also enriched in PGE, notably Pt and Pd, and the values of (Pt + Pd)/(Ru + Ir + Os) are up to fifteen times the value in the massive ore. Regarding the chalcopyrite veinlets, they occur widely throughout the deposit, cross-cutting most types of sulfide mineralization and silicate lithologies. However, they show very different (Pt + Pd)/(Ru + Ir + Os) values, depending upon the type of ore they cut, with higher values where they cross the Cu-rich disseminated mineralization.

These geochemical features suggest that the deposit is made up of ores with different degrees of fractionation and that the more fractionated Cu- and PGE-rich ores today lie along the southern margin of the southern mineralized body. The fractional crystallization of sulfide melts is a very common process in magmatic systems and has been extensively discussed by Naldrett *et al.* (1982, 1992, 1996, 1997) and Ebel & Naldrett (1996, 1997) for Noril'sk and Sudbury ore deposits. According to these authors, sulfide ore magmas differentiate on cooling, crystallizing a Ni-rich monosulfide solid-solution (*mss*) and concentrating Cu in the residual liquid. This liquid tends to escape from the solidified ore and forms chalcopyrite-bearing stringers adjacent to the previously crystallized ore. The PGE also are fractionated during this process: Os, Ir and Ru tend to remain in the Ni-rich fraction, whereas Rh and notably Pd and Pt are preferently concentrated within the Cu-rich fraction (Li *et al.* 1996, Barnes *et al.* 1997).

The Aguablanca massive and semimassive ore may thus represent a now re-equilibrated *mss* that crystallized at high temperature. The disseminated ore, with a lower Ni:Cu ratio (1–1.5) than that of the massive ore (2–5), is likely to represent small amounts of sulfide liquid that crystallized *in situ* while trapped in the crystallizing silicate magma. Regarding the Cu-rich disseminated sulfides, they are likely to have crystallized from a more fractionated sulfide liquid than the massive ore and the more typical disseminated ores, as indicated by their respective (Pt + Pd)/(Ru + Ir + Os) values. These Cu-rich disseminated ores are not likely to have been formed by the crystallization of the Cu-rich fraction remaining after the consolidation of the massive ores because the liquidus temperature of the silicate magma is higher than that of a fractionated sulfide liquid, and thus it would be difficult for a fractionated sulfide liquid to disperse to form disseminated ore in the solidified igneous rock. Such a Cu-rich ore, fractionated from the massive Ni-rich ore, is more likely to be injected in veins into the rocks surrounding the massive ore. The disseminated sulfides occurring in the southern part of the deposit thus likely crystallized from a different, more evolved, initial sulfide liquid that was richer in Cu and PGE than the sulfide magma that formed other parts of the deposit. Therefore, the Aguablanca sulfide mineralization may have formed by the emplacement of more than one magma and from different initial sulfide liquids with different degrees of fractionation, and not by the fractionation of a single sulfide melt. These sulfide liquids underwent fractional crystallization, and as a result, the sulfide droplets show separated Ni-rich and Cu-rich fractions (Fig. 8B), exemplifying this process on a small scale. The chalcopyrite veinlets may represent residual liquids enriched in Cu, Pd and Pt remaining after the consolidation of the *mss* and injected along fractures and grain boundaries in the solidified sulfide-rich silicate rocks. Their different (Pt + Pd)/(Ru + Ir + Os) values as they cut across different areas of sulfide ore may reflect their local origin from different initial sulfide liquids. Thus, the higher values of this ratio would correspond to veinlets related to the disseminated ore, richer in Cu, and with high values of (Pt + Pd)/(Ru + Ir + Os) (anal. 6 and 2, respectively, Table 5).

The breccias are hosted by massive ore, and they are likely to have formed at the magmatic stage. The presence of sulfides in the igneous matrix suggests that the brecciation event was coeval with the sulfide saturation

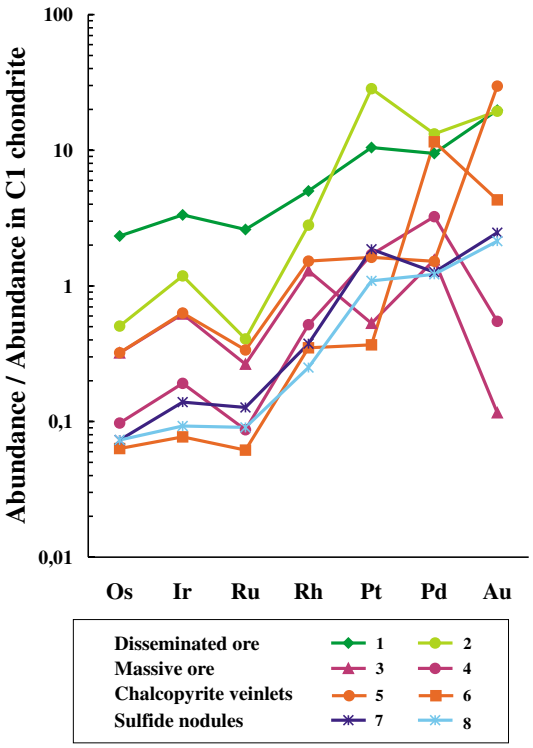

FIG. 15. Normalized patterns of PGE recalculated to 100% sulfides in different types of ore. The values used for chondrite normalization are those quoted by Naldrett & Duke (1980). Numbers refer to compositions in Table 5.

of the silicate magma and the subsequent crystallization and gravity settling of the sulfide liquids. In this sense, these magmatic breccias could be related to the emplacement of the sulfide-bearing units of the Aguablanca intrusion within the country rocks.

Postmagmatic evolution of the deposit

The postmagmatic evolution of the deposit involved two types of process: 1) development of a subsolidus re-equilibrated assemblage of sulfides, and 2) retrograde alteration of the host rocks and deposition of pyrite by skarn-related hydrothermal fluids. The timing of these processes cannot be precisely established, although they could have been partly coeval.

The pyrrhotite – pentlandite – chalcopyrite assemblage and textures, as they are observed now in the Aguablanca deposit, are the result of subsolidus re-equilibration during the cooling of the initially crystallized original magmatic sulfide liquid, *i.e.*, monosulfide and intermediate solid-solutions (the *mss* and *iss* fractions). The thermal conditions under which the exsolution processes took place in Aguablanca can be estimated from experimental work and other case studies (Kelly & Vaughan 1983, Hill 1984). Coarse crystals of pentlandite surrounding pyrrhotite initially exsolved within the pyrrhotite at temperatures in excess of 600°C and migrated later toward the edges of pyrrhotite grains. Diffusion rates were sufficiently rapid to allow segregation of the pentlandite into polycrystalline veinlets located on the edges of the pyrrhotite. Pentlandite showing flame textures resulted from exsolution at lower temperatures, down to 200°C. At these low temperatures, the rates of diffusion are apparently insufficient for the exsolving pentlandite to migrate to the grain boundaries of the pyrrhotite. According to experimental data (Hill 1984), chalcopyrite surrounding pyrrhotite may have been exsolved at temperatures of at least 600°C, together with earlier pentlandite, whereas the lamellae of chalcopyrite may correspond to late stages of exsolution, between 300° and 100°C.

The precipitation of pyrite, notably abundant in areas of strong microfracturing, is due to the circulation of postmagmatic fluids and took place during three distinct episodes (Py_1, Py_2 and Py_3, Fig. 9) under progressively decreasing temperature. These fluids could have been produced during reactions that formed the skarns developed at the expense of the Cambrian carbonate host-rocks as a consequence of the emplacement of the Aguablanca igneous body. The textural relationships between the euhedral megacrysts of pyrite (Py1) and the high-temperature exsolved pentlandite suggest that the circulation of fluids started very early in the postmagmatic history of the deposit and was broadly coeval with the subsolidus recrystallization of sulfides and the overall cooling of the deposit. Postmagmatic cooling and fluid circulation also induced the retrograde alteration of the igneous silicates in the mafic–ultramafic sequence, resulting in two assemblages: an early one with actinolite ± chlorite ± epidote ± albite ± serpentine (the latter mineral is only present in the ultramafic rocks), followed by talc ± chlorite ± carbonates.

Conditions of PGM formation

Within the context of this complex evolutionary history of the orebody, the conditions under which the PGM assemblage developed can be deduced from the current geochemical and textural features of the PGM. As presented above, the platinum-group minerals at Aguablanca mostly consist of bismuthotellurides, with michenerite and Pd-rich members of the merenskyite–moncheite solid-solution series as the main PGM. Experimental data in the Pd–Te–Bi system (Hoffman & MacLean 1976, Makovicky 2002) indicate that michenerite may crystallize only below 500°C, whereas merenskyite is stable up to 740°C, although variations in composition of the latter may modify this temperature. Thus, in the solid-solution series merenskyite–moncheite, the substitution of Pd for Pt increases the upper thermal limit of merenskyite, as moncheite can form up to 1150°C (Cabri 1981), whereas the substitution of Te for Bi strongly produces the opposite effect (Hoffman & MacLean 1976). At Aguablanca, the merenskyite–moncheite compositions (Fig. 12) range from Pt-free merenskyite to Pd-rich moncheite (Pt:Pd ≤ 2), and no examples of end-member moncheite have been found. This limited substitution of Pd for Pt indicates that the merenskyite did not approach the upper thermal limit of the solid-solution series during its formation. In addition, extensive substitution of Te for Bi is observed in these PGM, increasing from Pt-free merenskyite to Pt-bearing phases, thus suggesting that the effect of Pt could have been compensated by the introduction of Bi in the structure of these PGM. A temperature of crystallization of 400–450°C has been estimated for merenskyite lacking Pt (Fig. 13). This estimate is in agreement with the presence of michenerite in the PGM assemblage, either as individual crystals or as composite grains with other bismuthotellurides, as michenerite decomposes above 500°C (Hoffman & MacLean 1976).

These relatively low temperatures of crystallization indicate that the current PGM assemblage was generated during the retrograde evolution of the ore. Their textural relationships with the sulfides suggest that the PGM formed mostly as a result of subsolidus recrystallization of the ore; the circulation of hydrothermal fluids could have played a role only in restricted areas of the deposit. In the massive ore, most of the PGM occur enclosed within the magmatic sulfides (43% in pentlandite, 38% in pyrrhotite and 10% in chalcopyrite), and only 7% are located at the contact between minerals. The PGM also occur mainly within the sulfides in the disseminated ore, although up to 23% of the occurrences at sulfide–silicate grain boundaries is probably due to

the lower abundance of sulfides. In experimental studies on PGE solubility in base-metal sulfides, Makovicky *et al*. (1986) have found that pyrrhotite may dissolve substantial amounts of Pd and Pt at 900°C, but cooling down to 500°C and lower temperatures causes a sharp decrease in solubility, promoting the exsolution of PGE. The observed distribution of the PGM, combined with the experimental evidence, strongly suggest that the assemblage of PGM occurring within the massive sulfides exsolved during the low-temperature re-equilibration of the magmatic sulfide phases. The occurrence of Ni-bearing PGM (*i.e.*, palladian melonite), restricted only to the massive ore in which the exsolved pentlandite is more abundant, further supports this hypothesis.

In addition, some redistribution of the PGM related to the skarn processes in the nearby country-rocks and circulation of hydrothermal fluid cannot be ruled out. The occurrence of numerous bismuthotellurides of the PGE at grain boundaries in areas of massive sulfides with a high content of pyrite is significantly higher than that observed in areas where pyrite is absent (Fig. 11). This correlation suggests a migration of PGM to grain boundaries linked to fluid circulation in channelized areas in which pyrite was deposited. Nevertheless, PGM mobilization, if it occurred, took place at a grain scale, as most PGM remained within the sulfides where they previously exsolved, notably in the massive ore. The close association of the PGE bismuthotellurides with the magmatic sulfides, even in the disseminated ore, precludes a larger-scale remobilization and precipitation of PGE by hydrothermal fluids. This inference is further supported by the lack of PGM included in pyrite formed during any of the hydrothermal stages.

The PGM assemblage found in the gossan includes PGE oxides. These types of PGM have been described from both laterites and alluvial concentrations of PGE and have been observed only relatively recently in association with PGE-bearing layered and ophiolite complexes (*e.g.*, Nixon *et al*. 1990, Jedwab *et al*. 1993, Augé & Legendre 1994, Prichard *et al*. 1994, Moreno *et al.* 1999). They are considered to be the product of low-temperature alteration and surface weathering, either as a result of *in situ* alteration of earlier PGM or as precipitations from solution. Augé & Legendre (1994) attributed zoning in some of their PGE oxides to this process of precipitation. In the Aguablanca samples, the PGE oxides have been located in gossan samples taken from above PGE–sulfide mineralization. Relics of earlier, pre-gossan PGM surrounded by PGE oxides (or enclosed by them within euhedral pseudomorphs) show that the alteration of PGM to oxides occurred *in situ* by replacement rather than direct precipitation.

Acknowledgements

This work was made possible thanks to Atlantic Copper S.A., which provided information and drill-core samples from Aguablanca. We also acknowledge fruitful discussions with F. Gervilla (University of Granada) and comments made by A.J. Naldrett and E. Makovicky during the 31th International Geological Congress (Rio de Janeiro, 2000). The two reviewers, Dr. C. Farrow and notably Dr. Chusi Li, are especially acknowledged for their constructive comments, which greatly contributed to the improvement of the original manuscript. Wes Gibbons is gratefully acknowledged for help with the English version of the manuscript. This research has been financed by the DGCYT project (Spanish Ministry of Science and Technology).

References

Apalategui, O., Contreras, F. & Eguiluz, L. (1990): Santa Olalla del Cala. Memoria Explicativa de la Hoja 918. Mapa Geológico de España (Escala 1:50.000). Instituto Tecnológico Geominero de España, Madrid, Spain.

_____ & Sánchez Carretero, R. (1991): Síntesis y correlación de unidades en el borde meridional de la Zona de Ossa–Morena (ZOM): implicaciones geológicas. *Bol. Geol. Min*. **102**(3), 339-347.

Augé, T. & Legendre, O. (1994): Platinum-group element oxides from the Pirogues ophiolitic mineralization. New Caledonia: origin and significance. *Econ. Geol*. **89**, 1454-1468.

Barnes, S.-J., Makovicky, E., Makovicky, M., Rose-Hansen, J. & Karup-Møller, S. (1997): Partition coefficients for Ni, Cu, Pd, Pt, Rh, and Ir between monosulfide solid solution and sulfide liquid and the formation of compositionally zoned Ni–Cu sulfide bodies by fractional crystallization of sulfide liquid. *Can. J. Earth Sci.* **34**, 366-374.

Bateman, R., Martin, M.P. & Castro, A. (1992): Mixing of cordierite granitoid and pyroxene gabbro, and fractionation, in the Santa Olalla tonalite (Andalucia). *Lithos* **28**, 111-131.

Bomatí, O., Ortega, L., Lunar, R., Sierra, J., Moreno, T. & García Palomero, F. (1999): Distribución de sulfuros de Ni–Cu–Fe y de minerales del grupo del platino en la mineralización intramagmática de Aguablanca (Badajoz). Implicaciones genéticas. *Bol. Soc. Esp. Min.* **22-A**, 19-20.

Boyd, R. & Mathiesen, C.O. (1979): The nickel mineralization of the Råna mafic intrusion, Nordland, Norway. *Can. Mineral.* **17**, 287-298.

Bridges, J. C., Prichard, H. M., Neary, C. R. & Meireles, C. A. (1993): Platinum-group element mineralization in the chromite-rich rocks of the Braganca massif, northern Portugal. *Trans. Inst. Mining Metall.* **B 102**,103-113.

Cabri, L.J., ed. (1981): Platinum-Group Elements: Mineralogy, Geology, Recovery. *Can. Inst. Mining Metall., Spec. Vol.* **23**.

_____ (2002): The platinum-group minerals. *In* The Geology, Geochemistry, Mineralogy and Mineral Beneficiation

of Platinum-Group Elements (L.J. Cabri, ed.). *Can. Inst. Mining, Metall. Petroleum, Spec. Vol.* **54**, 13-129.

CASQUET, C. (1980): *Fenomenos de endomorfismo, metamorfismo y metasomatismo en los marmoles de la Ribera del Cala*. Ph.D. thesis, Universidad Complutense de Madrid, Spain.

_____, EGUILUZ, L., GALINDO, C., TORNOS, F. & VELASCO, F. (1998a): The Aguablanca Cu–Ni–(PGE) intraplutonic ore deposit (Extremadura, Spain). Isotope (Sr, Nd, S) contraints on the source and evolution of magmas and sulfides. *Geogaceta* **24**, 71-74.

_____, GALINDO, C., DARBYSHIRE, D.P.F. & NOBLE, S.R. (1998b): Fe–U–REE mineralization at Mina Monchi, Burguillos del Cerro, SW Spain: age and isotope (U–Pb, Rb–Sr and Sm–Nd) constraints on the evolution of the ores. *Geol. Assoc. Can. – Mineral. Assoc. Can. – APGGQ, Program Abstr.* **23**, A-28.

CASTRO, A., CORRETGÉ, L.G., DE LA ROSA, J., ENRIQUE, P., MARTÍNEZ, F.J., PASCUAL, E., LAGO, M., ARRANZ, E., GALÉ, C, FERNÁNDEZ, C., DONAIRE, T. & LÓPEZ, S. (2002): Palaeozoic magmatism. *In* The Geology of Spain (W. Gibbons & T. Moreno T., eds.). Geological Society, London, U.K. (117-153).

DALTRY, V.D.C. & WILSON, A.H. (1997): Review of platinum-group mineralogy: compositions and elemental associations of the PG-minerals and unidentified PGE-phases. *Mineral. Petrol.* **60**, 185-229.

DISTLER, V.V. & KUNILOV, V.E. (1994): *Geology and Ore Deposits of the Noril'sk Region*. Seventh Int. Platinum Symp. (Moscow), Field-Trip Guidebook.

EBEL, D.S. & NALDRETT, A.J. (1996): Fractional crystallization of sulfide ore liquids at high temperature. *Econ. Geol.* **91**, 607-621.

_____ & _____ (1997): Crystallization of sulfide liquids and the interpretation of ore composition. *Can. J. Earth Sci.* **34**, 352-365.

EGUILUZ, L., CARRACEDO, M. & APALATEGUI, O. (1989): Stock de Santa Olalla de Cala (Zona de Ossa Morena, España). *Stvd. Geol. Salaman.* **4**, 145-157.

_____, GIL IBARGUCHI, J.I., ABALOS, B. & APRAIZ, A. (2000): Superposed Variscan and Cadomian orogenic cycles in the Ossa–Morena zone and related areas of the Iberian Massif. *Geol. Soc. Am., Bull.* **112**, 1398-1413.

FARROW, C. E.G. & LIGHTFOOT, P.C. (2002): Sudbury PGE revisited: toward an integrated model. *In* The Geology, Geochemistry, Mineralogy and Mineral Beneficiation of Platinum-Group Elements (L.J. Cabri, ed.). *Can. Inst. Mining, Metall. Petroleum, Spec. Vol.* **54**, 273-297.

FORREST, M. (2003): Spanish surprise. *Materials World* **11**(9), 32-34.

FRIETSCH, R., PAPUNEN, H. & VOKES, F.M. (1979): The ore deposits in Finland, Norway and Sweden: a review. *Econ. Geol.* **74**, 975-1001.

GARUTI, G., FIANDRI, P. & ROSSI A. (1986): Sulphide composition and phase relations in the Fe–Ni–Cu ore deposits of the Ivrea–Verbano basic complex (western Alps, Italy). *Mineral. Deposita* **21**, 22-34.

_____ & RINALDI, R. (1986a): Melonite-group and other tellurides from the Ivrea–Verbano basic complex, western Italian Alps. *Econ. Geol.* **81**, 1213-1217.

_____ & _____ (1986b): Platinum-group and related minerals from the Ivrea–Verbano sulfide deposits. *Rend. Soc. Ital. Mineral. Petrol.* **41**(2), 229-244.

GERVILLA, F. & LEBLANC, M. (1990): Magmatic ores in high-temperature alpine-type lherzolite massifs (Ronda, Spain, and Beni Bousera, Morocco). *Econ. Geol.* **85**, 112-132.

_____, PAPUNEN, H., KOJONEN, K. & JOHANSON, B. (1998): Platinum-, palladium- and gold-rich arsenide ores from the Kylmäkoski Ni–Cu deposit (Vammala Nickel Belt, SW Finland). *Mineral. Petrol.* **64**, 163-185.

HÄKLI, T.A., VORMISTO, K. & HANNINEN, E. (1979): Vammala, a nickel deposit in layered ultramafite, southwest Finland. *Econ. Geol.* **74**, 1166-1182.

HARNEY, D.M.W. & MERKLE, R.K.W. (1990): Pt–Pd minerals from the Upper Zone of Eastern Bushveld Complex, South Africa. *Can. Mineral.* **28**, 619-628.

HAUCK, S.A., SEVERSON, M.J., ZANKO, L., BARNES, S.J., MORTON, P., ALMINAS, H., FOORD E.E. & DAHLBERG, E.H. (1997): An overview of the geology and oxide, sulfide and platinum-group element mineralization along the western and northern contacts of the Duluth Complex. *Geol. Soc. Am., Spec. Pap.* **312**, 137-195.

HILL, R.E.T. (1984): Experimental study of phase relations at 600°C in a portion of the Fe–Ni–Cu–S system and its application to natural sulfide assemblages. *In* Sulfide Deposits in Mafic and Ultramafic Rocks (D.L. Buchanan & M.J. Jones, eds.). Institution of Mining and Metallurgy, London, U.K. (14-21).

HOFFMAN, E. & MACLEAN, W.H. (1976): Phase relations of michenerite and merenskyite in the Pd–Bi–Te system. *Econ. Geol*. **71**, 1461-1468.

JEDWAB, J., CASSEDANNE, J., CRIDDLE, A.J., RY, P., GHYSENS, G., MEISSER, N., PIRET, P. & STANLEY, J. (1993): Rediscovery of palladinite PdO from Itabira (Minas Gerais, Brazil) and from Ruwe (Shaba, Zaire). *Terra Abstracts, Suppl. to Terra Nova 3* **5**, 22.

KELLY, D.P. & VAUGHAN, D.J. (1983): Pyrrhotite–pentlandite ore textures: a mechanistic approach. *Mineral. Mag*. **47**, 453-463.

LESHER, C.M. (2003): Metallogenesis of magmatic Ni–Cu–(PGE) deposits. *Can. Inst. Mining Metall., Annual Meeting* (*Montreal*).

_____ & KEAYS, R.R. (2002): Komatiite-associated Ni–Cu–(PGE) deposits: geology, mineralogy, geochemistry and genesis. *In* The Geology, Geochemistry, Mineralogy and Mineral Beneficiation of Platinum-Group Elements (L.J. Cabri, ed.). *Can. Inst. Mining, Metall., Petroleum, Spec. Vol*. **54**, 579-618.

LI, CHUSI, BARNES, S.-J., MAKOVICKY, E., ROSE-HANSEN, J. & MAKOVICKY, M. (1996): Partitioning of nickel, copper, iridium, rhenium, platinum and palladium between monosulfide solid solution and sulfide liquid: effects of composition and temperature. *Geochim. Cosmochim. Acta* **60**, 1231-1238.

LUNAR, R., GARCÍA PALOMERO, F., ORTEGA, L., SIERRA, J., MORENO, T. & PRICHARD, H. (1997): Ni–Cu–(PGM) mineralization associated with mafic and ultamafic rocks: the recently discovered Aguablanca ore deposit, SW Spain. *In* Mineral Deposits: Research and Exploration. Where Do They Meet? (H. Papunen, ed.). Balkema, Rotterdam, The Netherlands (463-466).

_____, MORENO, T., LOMBARDERO, M., REGUEIRO, M., LÓPEZ-VERA, F., MARTÍNEZ DEL OLMO, W., MALLO GARCÍA, J.M., SAENZ DE SANTA MARIA, J. A., GARCÍA-PALOMERO, F., HIGUERAS, P., ORTEGA, L. & CAPOTE, R. (2002): Economic and environmental geology. *In* The Geology of Spain (W. Gibbons & T. Moreno, eds.). Geological Society, London, U.K. (473-510).

MAKOVICKY, E. (2002): Ternary and quaternary phase systems with PGE. *In* The Geology, Geochemistry, Mineralogy and Mineral Beneficiation of Platinum-Group Elements (L.J. Cabri, ed.). *Can. Inst. Mining, Metall. Petroleum, Spec. Vol.* **54**, 131-175.

MAKOVICKY, M., MAKOVICKY, E. & ROSE-HANSEN, J. (1986): Experimental studies on the solubility and distribution of platinum group elements in base-metal sulfides in platinum deposits. *In* Metallogeny of Basic and Ultrabasic Rocks (M.J. Gallagher, R.A. Ixer, C.R. Neary C.R. & H.M. Prichard, eds.). The Intitution of Mining and Metallurgy, London, U.K. (415-425).

MARTÍN ESTÉVEZ, J.R., ORTEGA, L., LUNAR, R. & GARCÍA PALOMERO, F. (2000): Características texturales y geoquímicas de la pirita en la mineralización intramagmática de Ni–Cu–PGE de Aguablanca (Badajoz). *Cuad. Lab. Xeológico Laxe* **25**, 107-110.

MELEZHIK, V.A., HUDSON-EDWARDS, K.A., GREEN, A.H. & GRINENKO, L.I. (1994): The Pechenga area, Russia. 2. Nickel–copper deposits and related rocks. *Trans. Inst. Mining Metall., Section B, Appl. Earth Sci.* **103**, 146-161.

MISRA, K.C. & FLEET, M.E. (1973): The chemical composition of synthetic and natural pentlandite assemblages. *Econ. Geol.* **68**, 518-539.

MORENO, T., GIBBONS, W., PRICHARD, H. & LUNAR, R. (2001): Platiniferous chromitite and the tectonic setting of ultramafic rocks in Cabo Ortegal (north west Spain). *J. Geol. Soc. London* **158**, 601-614.

_____, PRICHARD, H., LUNAR, R., MONTERRUBIO, S. & FISHER, P. (1999): Formation of a secondary platinum-group assemblage in chromitites form the Herbeira ultramafic massif in Cabo Ortegal, NW Spain. *Eur. J. Mineral.* **11**, 363-378.

NALDRETT, A.J. (1999): World class Ni–Cu–PGE deposits: key factors in their genesis. *Mineral. Deposita* **34**, 227-240.

_____ & DUKE, J.M. (1980): Platinum metals in magmatic sulfide ores. *Science* **208**, 1417-1428.

_____, EBEL, D.S., ASIF, M., MORRISON, G. & MOORE, C.M. (1997): Fractional crystallisation of sulfide melts as illustrated at Noril'sk and Sudbury. *Eur. J. Mineral*. **9**, 365-377.

_____, FEDORENKO, V.A., ASIF, M., SHUSHEN, L., KUNILOV, V.E., STEKHIN, A.I., LIGHTFOOT, P.C. & GORBACHEV, N.S. (1996): Controls on the composition of Ni–Cu sulfide deposits as illustrated by those at Noril'sk, Siberia. *Econ. Geol.* **91**, 751-773.

_____, INNES, D.G., SOWA, J. & GORTON, M.P. (1982): Compositional variations within and between five Sudbury ore deposits. *Econ. Geol.* **77**, 1519-1534.

_____, LIGHTFOOT, P.C., FEDORENKO, V.A., GORBACHEV, N.S. & DOHERTY, W. (1992): Geology and geochemistry of intrusions and flood basalts of the Noril'sk region, USSR, with implications for the origin of the Ni–Cu ores. *Econ. Geol.* **87**, 975-1004.

NIXON, G.T., CABRI, L.J. & LAFLAMME, J.H.G. (1990): Platinum-group-element mineralization in lode and placer deposits associated with the Tulameen Alaskan-type complex, British Columbia. *Can. Mineral*. **28**, 503-535.

ORDOÑEZ, B., GEBAUER, D. & EGUILUZ, L. (1998): SHRIMP age-constraints for the calc-alkaline volcanism in the Olivenza–Monesterio antiform (Ossa Morena, SW Spain). *Program Goldschmidt Conf.* (*Toulouse*), *Abstr.*, 35.

ORTEGA, L., LUNAR, R., GARCÍA PALOMERO, F., MORENO, T. & PRICHARD, H. (2001): Removilización de minerales del grupo del platino en el yacimiento de Ni–Cu–EGP de Aguablanca (Badajoz). *Bol. Soc. Esp. Min.* **24-A**, 175-176.

_____, MORENO, T., LUNAR, R., PRICHARD, H., SIERRA, J., BOMATÍ, O., FISHER, P. & GARCÍA PALOMERO, F. (1999): Minerales del grupo del platino y fases asociadas en el depósito de Ni–Cu–EGP de Aguablanca, SW España. *Geogaceta* **25**, 155-158.

_____, PRICHARD, H., LUNAR, R., GARCÍA PALOMERO, F., MORENO, T. & FISHER, P. (2000): The Aguablanca discovery. *Mining Mag*. **2**, 78-80.

OSCHSNER, A. (1993): *U–Pb Geochronology of the Upper Proterozoic - Lower Paleozoic Geodynamic Evolution in the Ossa Morena Zone (SW Iberia): Constraints on the Timing of the Cadomian Orogeny*. Ph.D. dissertation, Eidgenössische Technische Hochschule, Zürich, Switzerland.

PRICHARD, H., IXER, R.A., LORD, R.A., MAYNARD, J. & WILLIAMS, N. (1994): Assemblages of platinum-group minerals and sulfides in silicate lithologies and chromite-rich rocks within the Shetland ophiolite. *Can. Mineral*. **32**, 271-294.

QUESADA, C. (1992): Evolución tectónica del Macizo Ibérico (Una historia de crecimiento por acrecencia sucesiva de terrenos durante el Proterozoico superior y el Paleozoico). *In* Paleozoico Inferior de Ibero-América (J.C. Gutiérrez Marco, J. Saavedra, J. & I. Rábano, eds.). Junta de Extremadura, Mérida, Spain (173-190).

_____ (1996): Evolución geodinámica de la zona de Ossa Morena durante el ciclo Cadomiense. *In* Estudos sobre a geología da Zona de Ossa Morena (Maciço Ibérico) (A. Araujo & M.F.C. Pereira, eds.). Univ. Evora, Evora, Portugal (205-230).

SÁNCHEZ CARRETERO, R., EGUILUZ, L., PASCUAL, E. & CARRACEDO, M. (1990): Igneous rocks of the Ossa Morena Zone. *In Premesozoic Geology of Iberia* (R.D. Dallmeyer & E. Martínez García, eds.). Springer Verlag, Heidelberg, Germany (292-313).

SÁNCHEZ GARCÍA, T., BELLIDO, F. & QUESADA, C. (2003): Geodynamic setting and geochemical signatures of Cambrian-Ordovician rift-related igneous rocks (Ossa-Morena Zone, SW Iberia). *Tectonophysics* **365**, 233-255.

STUMPFL, E.F. (1961): Some new platinoid-rich minerals, identified with the electron micro-analyser. *Mineral. Mag*. **32**, 833-847.

TORNOS, F., CASQUET, C., GALINDO, C., CANALES, A, & VELASCO, F. (1999): The genesis of the Variscan ultramafic-hosted magmatic Cu–Ni deposit of Aguablanca, SW Spain. *In* Mineral Deposits: Processes to Processing (C.J. Stanley *et al.*, eds.). Balkema, Rotterdam, The Netherlands (795-798).

_____, _____, _____, VELASCO, F. & CANALES, A. (2001): A new style of Ni–Cu mineralization related to magmatic breccia pipes in a transpressional magmatic arc, Aguablanca, Spain. *Mineral. Deposita* **36**, 700-706.

VALLADARES, M. I., BARBA, P. & UGIDOS, J. (2002): Precambrian. *In* The Geology of Spain (W. Gibbons & T. Moreno T., eds.). Geological Society, London, U.K. (7-16).

Received July 23, 2001, revised manuscript accepted November 9, 2003.